Plasmodesmal closure elicits stress responses

Author names and affiliations: Estee E. Tee[1,†], Andrew Breakspear[1,†], Diana Papp[1,2,†], Hannah R. Thomas[1,3], Catherine Walker[1], Annalisa Bellandi[1,4], Christine Faulkner[1]

[1]Cell and Developmental Biology, John Innes Centre, Norwich Research Park, Norwich, NR4 7UH, UK
[2]Present address: Department of Metabolism, Digestion and Reproduction, Imperial College London, London, W12 0NN, UK
[3]Present address: Department of Horticulture, Zijingang Campus, Zhejiang University, Hangzhou, China
[4]Present address: Laboratoire de Reproduction et Développement des Plantes, École Normale Supérieure de Lyon, 69342 Lyon, France
[†]These authors contributed equally to this work
Corresponding author: Christine Faulkner

Abstract

Plant cells are connected to their neighbors via plasmodesmata facilitating the exchange of nutrients and signaling molecules. During immune responses, plasmodesmata close, but how this contributes towards a full immune response is unknown. To investigate this, we developed two transgenic lines with which we could induce plasmodesmal closure independently of immune elicitors, using the over-active CALLOSE SYNTHASE3 allele *icals3m* and the C-terminus of PDLP1 to drive callose deposition at plasmodesmata. Induction of plasmodesmal closure increased the expression of stress responsive genes, salicylic acid accumulation and resistance to *Pseudomonas syringae* DC3000. More homogeneous plasmodesmal closure using *icals3m* also led to the accumulation of starch and sugars, decreased leaf growth, as well as hypersusceptibility to *Botrytis cinerea*. Based on the profile of responses, we conclude that plasmodesmal closure itself activates stress signaling, raising questions of what signals mediate this response and whether these responses occur in all circumstances when plasmodesmata close.

Keywords: plasmodesmata / defense / callose / stress signaling

38 **Introduction**

39 Plants are multicellular organisms, with almost every plant cell cytoplasmically
40 connected to its neighbors. While most plant cells are equipped with machinery to
41 respond autonomously to a range of stress signals, optimal responses involve the
42 regulation of this cytoplasmic connectivity between cells. This is particularly evident in
43 immune signaling; most cells produce the receptors that perceive microbial threats
44 and can activate appropriate responses, but the degree of connectivity to neighboring
45 cells is a critical part of the full immune response (Lee et al. 2011; Faulkner et al.
46 2013). Indeed, if plants cannot regulate the cytoplasmic connectivity between cells,
47 they are more susceptible to infection by a range of pathogenic microbes. Despite this
48 observation, we don't yet understand how cell-to-cell connectivity contributes to an
49 overall immune response.

50 Cytoplasmic connectivity between plant cells is established via membrane-lined
51 bridges called plasmodesmata. Plasmodesmata are dynamic structures and the
52 oscillation in their aperture, i.e., closing and opening, allows control over the flux of
53 soluble molecules between cells. We broadly assume that many molecules that move
54 through plasmodesmata, including plant hormones, mRNAs, and proteins, are
55 information carriers and that aperture changes thus impact cell-to-cell communication.
56 Indeed, if an immune response involves the production of soluble defense-associated
57 molecules, their passage through plasmodesmata could transmit critical information
58 to neighboring (or distant) naïve cells.

59 Plant immune responses include a decrease in plasmodesmal aperture, which
60 reduces cell-to-cell movement of molecules (as recently reviewed by Wang et al.
61 2021b; German et al. 2023; Alazem and Burch-Smith 2024). Plasmodesmal aperture
62 is regulated via callose deposition and degradation at the plasmodesmal neck by
63 callose synthases (CalS) and β-glucanases respectively (Levy et al. 2007; Vatén et al.
64 2011). The decrease in plasmodesmal aperture in response to stress is a process
65 activated by signaling cascades mediated by specific machinery. For example, LYSM-
66 CONTAINING GPI-ANCHORED PROTEIN 2 (LYM2; Faulkner et al. 2013) and
67 CALMODULIN-LIKE 41 (CML41; Xu et al. 2017) specifically mediate plasmodesmal
68 responses to the microbial elicitors chitin and flg22 respectively, and
69 PLASMODESMATA LOCATED PROTEIN 5 (PDLP5) integrates these responses, as

well as plasmodesmal responses triggered by the defense hormone salicylic acid (SA; Wang et al. 2013; Tee et al. 2023b). The observation that *lym2* mutants cannot close their plasmodesmata in response to chitin but execute normal chitin-triggered mitogen-activated protein kinase (MAPK) activation and apoplastic ROS production (Faulkner et al. 2013) indicates that plasmodesmal signaling cascades can act independently of other immune responses. This independence of response suggests that whether plasmodesmata are open or closed might be informed by another layer of cellular regulation.

It has been observed that plasmodesmal permeability decreases upon PAMP perception within 30 min (Xu et al. 2017) and is still detected after 24 hours (Lim et al. 2016; Li et al. 2021). Both PAMP perception and pathogen infection initiate a wide array of defense responses making it challenging to identify the specific contribution of plasmodesmal closure to immunity. Further, in the context of an infection, many pathogens deploy effectors targeting plasmodesmata that suppress plasmodesmal closure (e.g. Aung et al, 2020; Tomczynska et al. 2020; Li et al. 2021; Ohtsu et al. 2024), further complicating the analysis of the role of plasmodesmata in host immune execution in an infection context.

Whether plasmodesmata can close or not during immune responses determines whether a full defense response can be executed but untangling how plasmodesmal closure contributes to overall immunity is a complex problem. To begin to address this we have simplified the question and asked what cellular responses are triggered by plasmodesmal closure, and how closing plasmodesmata affects elements of an immune response. We generated two genetic tools with which we can induce plasmodesmal closure independently of an immune or stress elicitor. By identifying what responses are trigged by plasmodesmal closure in both tools, we found that plasmodesmal closure itself instigates a subset of stress responses including transcriptional reprogramming and salicylic acid (SA) production. This raises further questions regarding how this contributes to the orchestration of immune responses, how plasmodesmal closure triggers stress responses and whether these stress responses occur during the broad range of physiological processes during which plasmodesmata close.

Results

102 *Genetic tools induce plasmodesmal closure independent of a physiological elicitor*

103 To manipulate plasmodesmal closure independently of external signals we generated
104 two transgenic lines in which estradiol application can induce callose deposition at
105 plasmodesmata. First, we exploited the *icals3m* overactive *CalS3* allele (Vatén et al.
106 2011) that enhances callose deposition at plasmodesmata; *icals3m* has been used
107 extensively as a tool to understand symplastic connection in development (e.g.,
108 Paterlini et al. 2021; Ross-Elliott et al. 2017; Sevilem et al. 2012; Wu et al. 2016; Yadav
109 et al. 2014) but less is known about its effect on immunity. As a callose synthase, this
110 enzyme acts terminally in the plasmodesmal-associated callose deposition pathway.
111 Secondly, we utilized the observation that a synthetic construct of the fluorescent
112 protein mCherry fused between the PDLP1 signal peptide, and the PDLP1
113 transmembrane domain and cytoplasmic tail, also promotes callose deposition at
114 plasmodesmata (Caillaud et al. 2014). We fused these two transgenes independently
115 to the *XVE* chimeric transcription activator and *LexA* operator (Zuo et al. 2000) and
116 transformed them into *Arabidopsis thaliana* Col-0 to create two different inducible
117 tools, named LexA::icals3m and LexA::PD-Plug respectively. To identify functional
118 transgenic lines, we performed qPCR, copy number analysis and/or live imaging
119 (Supplemental Table 1; Supplemental Fig. S1).

120 To functionally characterize the selected LexA::PD-Plug and LexA::icals3m lines, we
121 first measured callose deposition by quantitative live cell imaging of aniline blue
122 stained plasmodesmal callose 24 hours (h) post estradiol treatment. At this timepoint,
123 both LexA::PD-Plug and LexA::icals3m showed greater accumulation of callose at PD
124 when compared to the DMSO treatment, although there was a greater response in
125 LexA::icals3m (Fig. 1a; Supplemental Fig. S2) suggesting that this line can deposit
126 more callose at plasmodesmata than LexA::PD-Plug. To determine whether increased
127 callose deposition perturbed plasmodesmal permeability, we used microprojectile
128 bombardment assays of *35S::GFP* to measure GFP flux between cells in DMSO or
129 estradiol treated leaves. While estradiol treatment did not impact GFP flux in
130 comparison to DMSO in wild-type Col-0 plants, we found that estradiol induction of
131 either transgene reduced GFP flux between cells, indicating plasmodesmal aperture
132 was reduced and cell-to-cell connectivity decreased (Fig. 1b-c; Supplemental Data Set
133 1). The extent of GFP flux was significantly less in induced LexA::icals3m compared
134 to induced LexA::PD-Plug (Fig. 1c). From these results, we conclude that estradiol

135 induces plasmodesmal callose deposition, and plasmodesmal closure in both
136 LexA::PD-Plug and LexA::icals3m, but not Col-0.

137 We noted that the data obtained from GFP mobility assays indicates that induced
138 LexA::PD-Plug displays heterogeneous plasmodesmal closure; while there is an
139 increase in the population of cells that exhibit plasmodesmal closure in induced
140 tissues, a subset of the population of cells remain connected to their neighbors (Fig.
141 1c; Supplemental Fig. S3). This is reminiscent of the data obtained from GFP mobility
142 assays of leaves treated with elicitors such as chitin and flg22 (Cheval et al. 2020; Tee
143 et al. 2023). By comparison, induced LexA::icals3m displays a more homogenous
144 response in which low variance in cell-to-cell movement is observed (Fig. 1c;
145 Supplemental Fig. S3), similar to transgenic lines such as the PDLP1-overexpressor
146 (Tee et al. 2023).

147 To further characterize the selected LexA::PD-Plug and LexA::icals3m lines, we
148 profiled the timing of plasmodesmal callose deposition across an extended timeline.
149 Significant plasmodesmal callose accumulation following estradiol treatment was first
150 detected at 24 h post treatment in both LexA::PD-Plug and LexA::icals3m, and was
151 sustained up to 72 h post treatment (Supplemental Fig. S4). Despite differences in the
152 degree of plasmodesmal closure, these transgenic lines allow us to manipulate
153 plasmodesmata independently of both endogenous and non-endogenous signals and
154 investigate plant responses to plasmodesmal closure.

155

156 *Plasmodesmal closure triggers stress transcriptional responses and salicylic acid*
157 *production*

158 As pathogens are capable of manipulating plasmodesmal aperture during infection, it
159 is difficult to determine whether plants sustain immune-associated plasmodesmal
160 closure when challenged with a pathogen over time. Thus, we examined callose
161 deposition in response to infection by *Pseudomonas syringae* DC3000 (*Pst* DC3000)
162 mutant strain *hrcC*$^{-}$ that does not secrete effectors that manipulate plasmodesmal
163 aperture. We found that plasmodesmal callose was deposited throughout the leaf at
164 24 h, 48 h and 72 h post infection (hpi), and significantly increased at 48 and 72 hpi
165 (Supplemental Fig. S5). This indicates that sustained plasmodesmal closure occurs
166 throughout an infection context.

167 To investigate the impact of sustained plasmodesmal closure on leaf tissue, we next
168 characterized the transcriptional profile of this process using RNAseq, identifying
169 transcriptional changes at 12 h, 24 h, 48 h and 72 h following DMSO or estradiol
170 treatment in LexA::icals3m and LexA::Plug. Preliminary analysis of the data first
171 revealed that a critical driving factor of variance was time (Supplemental Fig. S6).
172 Therefore, all subsequent analyses were performed within single time points. We
173 assessed the effect of estradiol relative to DMSO treatment within a genotype,
174 identifying differentially expressed genes (DEGs). The greatest response was in Col-
175 0 at 12 h, where estradiol led to the downregulation of over a thousand genes
176 (Supplemental Fig. S7). We checked whether estradiol influenced plasmodesmal
177 associated callose deposition in Col-0, but no change was detected (Supplemental
178 Fig. S8). The presence of shared estradiol-responsive DEGs in Col-0 and the
179 transgenic genotypes supports the possibility of an early estradiol specific response
180 not correlated to transgene induction. The number of these shared estradiol-induced
181 DEGs detected was dramatically reduced after 24 h (Supplemental Data Set 2;
182 Supplemental Fig. S7), suggesting secondary transcriptional effects of estradiol are
183 negligible after this point.

184 To further validate our tools, we assessed the transgene induction across the sampling
185 period; both PD-Plug transcripts (as indicated by read counts of mCherry) and icals3m
186 transcripts (as indicated by read counts of CalS3) were upregulated compared to
187 controls by 12 h post estradiol treatment and remained significantly elevated at 72 h
188 (Supplemental Fig. S9). Specifically, the PD-Plug transgene was induced to a level
189 comparable to other highly expressed genes such as photosynthetic gene *RBCS1A*
190 (AT1G67090; Supplemental Data Set 3). To determine that the upregulation of the
191 transgenes did not induce ER stress from high levels of ectopic protein production, we
192 examined the expression of genes known to be ER stress markers, defined as either
193 ER stress sensors or unfolded protein response (UPR) effectors (Beaugelin et al.
194 2020). Of the 13 genes examined, only *BIP3* (AT1G09080) was significantly
195 upregulated in estradiol treated LexA::PD-Plug and LexA::icals3m at 72 h
196 (Supplemental Fig. S10), suggesting that transgene expression in these lines does not
197 induce ER-stress. We also investigated gene expression changes specific to the
198 induction of each transgene by using a likelihood-ratio test (Supplementary Data Set
199 4; Supplemental Fig. S11). At both 12 h and 24 h, we found no genes uniquely

200 upregulated in the estradiol treated samples from either LexA::PD-Plug or
201 LexA::icals3m. At 48 h, 28 and five genes were uniquely upregulated in estradiol
202 treated LexA::PD-Plug and estradiol treated LexA::icals3m respectively. At 72h, 33
203 genes were differentially upregulated in estradiol treated LexA::icals3m alone; there
204 were no genes differentially upregulated exclusively in estradiol treated LexA::PD-Plug
205 at 72 h.

206 While both the *icals3m* and *PD-Plug* transgenes have different modes of action as
207 proteins, we reasoned that the genes that are commonly up- or down-regulated
208 following induction are associated with their common effect on plasmodesmata and
209 likely to indicate core responses to plasmodesmal closure. To identify genes uniquely
210 upregulated when plasmodesmata are closed, we defined two different groups for
211 comparison: plasmodesmal state closed (estradiol treated LexA::PD-Plug and
212 LexA::icals3m) and plasmodesmal state open (DMSO treated LexA::PD-Plug and
213 LexA::icals3m, and all Col-0 samples). A likelihood-ratio test was performed on these
214 two groupings at each time point to identify genes that were significantly differentially
215 expressed only in the closed plasmodesmal state (Fig. 2a; Supplemental Fig. S12;
216 Supplemental Data Set 5-8) and observed that the number of upregulated DEGs
217 increased over time, suggesting that the longer plasmodesmata remain closed, the
218 greater the cellular response. Notably, the number of differentially expressed genes
219 that was shared between LexA::icals3m and LexA::PD-Plug in the grouping of
220 plasmodesmal state closed was greater than the number of up-regulated DEGs
221 specific to each line (Fig. 2a). A GO term analysis identified that genes upregulated
222 when plasmodesmata are closed at 48 and 72 h are enriched in defensive processes
223 (Fig. 2b; Supplemental Fig. S13). These include response to bacterium, oomycetes,
224 chitin and fungus, regulation of systemic acquired resistance, and response to salicylic
225 acid (SA).

226 As response to SA at 72 h was the most significantly enriched GO term in the entire
227 analysis, we further explored this by analyzing DEGs related to SA to determine what
228 aspects of SA signaling were impacted when plasmodesmata were closed (Fig. 2c;
229 see Supplemental Data Set 9 for associated references; Vlot et al. 2008; Seyfferth et
230 al. 2014; Yang et al. 2015; van Butselaar and Van den Ackerveken 2020) and found
231 both SA biosynthesis/catabolism and SA response pathways were significantly
232 upregulated at 48 and 72 h. To confirm that the transcriptional signature of SA is a

233 consequence of the activation of SA synthesis when plasmodesmata are closed, we
234 measured SA content in Col-0, LexA::PD-Plug and LexA::icalsm3 72 h post DMSO
235 and estradiol treatment. We found induced plasmodesmal closure increased SA
236 content in both LexA::PD-Plug and LexA::icals3m, with induced LexA::icals3m having
237 a greatly increased SA content, being three-fold higher when compared to DMSO
238 treatment (Fig. 2d). Previous studies have shown pathogen-induced SA accumulation
239 is associated with the suppression of jasmonic acid (JA) signaling (e.g. Spoel et al.
240 2003). While GO terms associated with JA signaling and response were enriched
241 amongst DEGs associated with 48 and 72 h PD closure (Fig. 2b, Supplemental Fig.
242 S14), we could not quantify any differences in JA content in tissue when PD were
243 closed (Supplemental Fig. S14). Overall, plasmodesmal closure leads to the
244 upregulation of transcriptional defense responses, and SA synthesis and
245 accumulation, independent of an immune stimulus.

246

247 *Plasmodesmal closure differentially impacts pathogen resistance and immune*
248 *responses*

249 Plants that lack plasmodesmata-specific immune signaling machinery and cannot
250 close their plasmodesmata in response to pathogen infection, show increased
251 susceptibility to different pathogenic microbes (Lee et al. 2011; Faulkner et al. 2013;
252 Xu et al. 2017). To determine whether an inverse correlation exists for induced
253 plasmodesmal closure we examined the susceptibility of induced, transgenic lines to
254 the bacterial, biotrophic pathogen *Pst* DC3000. We inoculated expanded leaves of
255 Col-0, LexA::PD-Plug and LexA::icals3m plants 72 h post DMSO or estradiol treatment
256 (Fig. 3a) and found that induction of both transgenes reduced bacterial growth 3 days
257 post infection (dpi). Thus, plasmodesmal closure is correlated with enhanced
258 resistance to *Pst* DC3000. Next, we assayed for resistance to the fungal necrotroph,
259 *Botrytis cinerea*. In contrast with *Pst* DC3000 infection, we found induction of the PD-
260 Plug transgene had no impact on *B. cinerea* infection when compared to the disease
261 caused in Col-0 plants, but induction of *icals3m* increased susceptibility to *B. cinerea*
262 (Fig. 3b; Supplemental Fig. S15). This indicates that plasmodesmal closure
263 specifically does not enhance resistance in all infection contexts.

264 Overall susceptibility is driven by multiple components of host defense responses, and
265 plasmodesmal closure is a key immune response to the pathogen associated
266 molecular patterns (PAMPs) flg22 and chitin. To determine if plasmodesmal closure
267 in our transgenic lines influences other PAMP responses, we assessed the activation
268 of MAPK signaling and ROS production by flg22 in induced LexA::icals3m and
269 LexA::Plug. When we assayed for flg22-triggered MAPK phosphorylation in mature
270 leaves and seedlings of both lines following estradiol treatment, we saw no difference
271 in the timing or magnitude of the response when compared to Col-0 (Fig. 3c;
272 Supplemental Fig. S16). By contrast, while induction of *LexA::PD-Plug* did not perturb
273 the flg22-triggered ROS burst in either mature leaves or seedlings (Fig. 3d,e), when
274 we assayed for the same response in LexA::icals3m, induction of the transgene
275 reduced the flg22-triggered ROS burst in mature leaves (Fig. 3d) and increased the
276 response in seedlings (Fig. 3e). To determine whether there were differences in
277 general basal cellular ROS levels that might explain this observation, we stained
278 estradiol treated Col-0 and LexA::icals3m leaves with H_2DCFDA but observed no
279 quantitative differences between the genotypes or treatments (Supplemental Fig.
280 S17), indicating plasmodesmal closure itself does not alter basal ROS cellular levels.

281 These results indicate that plasmodesmal closure differentially influences the
282 outcomes of host interactions with different pathogenic microbes, possibly correlated
283 with differences in pathogen lifestyle. Increased resistance to *Pst* DC3000 is not
284 associated with enhanced MAPK activation or, given that our pathoassays were
285 performed on mature leaves, changes in ROS burst responses. Further, our ROS data
286 raises the possibility that plasmodesmal closure differentially interacts with immune
287 responses in different developmental stages.

288

289 *Plasmodesmal closure induces sugar accumulation and growth defects*

290 As plasmodesmata connect the phloem to cells in young sink tissues and allow sugar
291 translocation, we expect that plasmodesmal closure might reduce the flux of sugars to
292 growing tissues and limit growth. Alternatively, activation of defense processes can
293 negatively regulate growth and therefore it is possible that plasmodesmal closure
294 impairs growth by one or both pathways. Indeed, several transgenic lines known for
295 constitutive plasmodesmal closure such as *PDLP1, PDLP5* and *PDLP6*

296 overexpressors (Thomas et al. 2008; Lee et al. 2011; Li et al. 2024) exhibit a significant
297 retardation in growth. Thus, we explored whether sustained plasmodesmal closure
298 reduced growth in induced LexA::PD-Plug and LexA::icals3m. In 9-day old seedlings,
299 we applied either DMSO or estradiol treatment and measured the first true leaves (Fig.
300 4a) six days post treatment. We found that while estradiol reduced leaf growth in both
301 Col-0 and LexA::PD-Plug in comparison to the DMSO treated seedlings, the estradiol-
302 induced growth reduction was greater in LexA::icals3m relative to LexA::PD-Plug and
303 Col-0. Alongside reduced leaf size, we observed yellowing and chlorosis on the
304 cotyledons of estradiol treated LexA::icals3m (Supplemental Fig. S18).

305 Plasmodesmal closure might be expected to restrict photoassimilate distribution
306 between source and sink tissue; a reduction in plasmodesmal permeability and rosette
307 size has been documented in *Arabidopsis* alongside a significant accumulation of
308 soluble sugars and starch (e.g., in the MOVEMENT PROTEIN 17 *MP17*
309 overexpressor, *CHOLINE TRASPORTER-LIKE 1 cher1* mutant, *PDLP5* and *PDLP6*
310 overexpressors; Kronberg et al. 2007; Kraner et al. 2017; Li et al. 2024). Therefore,
311 we quantified sugar accumulation in source tissues following plasmodesmal closure,
312 measuring the sucrose, fructose, glucose, and starch content of source leaves of
313 plants 72 h post treatment. These data reveal a significant increase in all four sugars
314 in estradiol treated LexA::icals3m samples (Fig. 4b). Reasoning that an increase in
315 sugar content might down-regulate photosynthesis, we used chlorophyll fluorescence
316 imaging to infer photosynthetic yield and found there was no difference in
317 photosynthetic yield of PSII (as indicated by Y(II)) after 72 h in Col-0, LexA::PD-Plug
318 and LexA::icals3m between the DMSO or estradiol treatments (Table 1). As there were
319 no changes in the photosynthetic yield that correlated with the increase in sugar
320 content in induced LexA::icals3m, we next hypothesized that plasmodesmal closure
321 and sugar accumulation might activate the expression of sugar transporters and starch
322 biosynthesis genes to reduce the concentration of soluble sugars in the cytosol.
323 However, out of 125 genes known to be sugar and starch related (Supplemental Data
324 Set 10; Büttner and Sauer 2000; Williams et al. 2000; Chen et al. 2010; Monroe and
325 Storm 2018; Abt and Zeeman 2020; Preiser et al. 2020; Smith and Zeeman 2020;
326 David et al. 2022; Bavnhøj et al. 2023), only the transporter *SENESCENCE-*
327 *ASSOCIATED GENE 29 (SAG29)/SUGARS WILL EVENTUALLY BE EXPORTED*
328 *TRANSPORTERS 15 (SWEET15)* was significantly upregulated when

329 plasmodesmata are closed, in LexA::icals3m at 48h and 72 h (Supplemental Fig. S19,
330 S20). AT3G20460 was differentially expressed in LexA::icals3m estradiol treatment at
331 72 h and is proposed to be a monosaccharide transporter (Johnson et al. 2006).
332 However, this gene was downregulated in response to plasmodesmal closure and as
333 the function of this gene is not yet well characterized it is difficult to speculate on any
334 possible role in the sugar/starch phenotype (Johnson et al. 2006). These results
335 indicate that while plasmodesmal closure induces starch and soluble sugar
336 accumulation, it does not perturb photosynthesis or the expression of sugar
337 transporters.

338 We reasoned that sugar accumulation might induce osmotic stress and so to test
339 whether sugar accumulation impairs growth and induces senescence in
340 LexA::icals3m, we simultaneously induced plasmodesmal closure and lowered the
341 light intensity by shading the plants to reduce photosynthesis and thus starch and
342 sugar content (Law et al. 2018). We observed that shade conditions reduced growth
343 in all plants, even Col-0, compared to the light grown plants after 14 days of this light
344 regime (Supplemental Fig. S21). However, estradiol treatment of LexA::icals3m had a
345 further size reduction in comparison to the DMSO treatment (Fig. 4c). While
346 senescence of cotyledons was still evident, it was not as severe as that induced in
347 normal light conditions (Supplemental Fig. S21). This suggests that while
348 plasmodesmal closure induces starch and sugar accumulation, this does not impair
349 growth or singularly induce senescence, and that these phenotypes are regulated by
350 other consequences of plasmodesmal closure.

351

352 *SA does not mediate plasmodesmal-induced effects on growth and resistance*

353 Given we detected that plasmodesmal closure increases SA and this could induce the
354 observed senescence and reduction in growth in LexA::icals3m, we sought to test if
355 there is a causal relationship. To test the hypothesis that SA accumulation reduces
356 size and/or induces senescence, we crossed LexA::icals3m with plants that
357 constitutively express *NahG*, the bacterial SA hydroxylase that degrades SA (Gaffney
358 et al. 1993; Delaney et al. 1994; Friedrich et al. 1995; NahG×icals3m). We observed
359 a significant reduction in leaf size as well as senescence observed in the cotyledons
360 after 14 days post plasmodesmal closure in both LexA::icals3m and NahG×icals3m

361 plants (Fig. 4c and Supplemental Fig. S21), indicating that SA accumulation is not the
362 cause of these phenotypes. Like LexA::icals3m, NahG×icals3m plants showed
363 reduced growth and mild cotyledon senescence when grown in shade conditions,
364 suggesting that SA does not contribute to the effects of plasmodesmal closure
365 observed in these conditions.

366 Lastly, we utilized the NahG×icals3m cross to investigate whether plasmodesmal
367 closure enhances pathogen resistance to *Pst* DC3000 by accumulation of SA. We
368 inoculated LexA::icals3m and NahG×icals3m plants 72 h post DMSO or estradiol
369 treatment (Fig. 4d) and found DMSO treated NahG×icals3m had the highest level of
370 bacterial growth 3 days post infection (dpi). However, estradiol treatment of both
371 LexA::icals3m and NahG×icals3m reduced bacterial growth suggesting that SA
372 accumulation is not the primary cause of the increased resistance induced by
373 plasmodesmal closure.

374 **Discussion**

375 Plants initiate a suite of defense responses when challenged by a microbial threat.
376 Plasmodesmal closure is an early reaction, initiated within 30 minutes of perceiving
377 pathogen-derived molecules and stress-associated signals including SA and
378 hydrogen peroxide (Xu et al. 2017; Cheval et al. 2020; Tee et al. 2023b), and is critical
379 for the execution of a full response. Thus, we reason that plasmodesmal closure
380 regulates a range of downstream processes. However, considering the plethora of
381 responses elicited during immunity, and the array of elicitors that trigger plasmodesmal
382 closure via converging signaling pathways (Tee et al. 2023b), it is challenging to
383 identify what specific contribution plasmodesmal closure makes to the overall
384 execution of immunity. Using lines with which we can induce plasmodesmal closure
385 independently of biotic elicitors, we explored what occurs when plasmodesmata close
386 without other co-incident processes and determined that plasmodesmal closure itself
387 induces stress.

388 Transcriptional profiling of responses to plasmodesmal closure identified
389 transcriptional signatures of defense responses associated with SA production and
390 signaling. It has long been known that constitutive over-production of the
391 plasmodesmal protein PDLP5 closes plasmodesmata and leads to high levels of SA
392 (Wang et al. 2013). However, as *PDLP5* transcriptionally responds to SA, it is viewed

393 as a stress response element (Wang et al. 2013). We have previously shown that
394 microbial elicitors, flg22 and chitin, also require PDLP5 to elicit plasmodesmal closure
395 (Tee et al. 2023b) posing a potential model in which plasmodesmal closure is first
396 initiated upon pathogen perception, leading to the accumulation of SA at
397 plasmodesmata to create a feedback loop to sustain closure.

398 The accumulation of SA when plasmodesmata are closed might be elicited directly or
399 indirectly. SA accumulates to higher levels in induced LexA::icals3m (Fig. 2d), in
400 parallel with an increase in sugars (Fig. 4c) and correlated with greater plasmodesmal
401 closure observed in this line relative to LexA::PD-Plug (Fig. 1c). It is possible that the
402 increase in sugar content induces osmotic stress or another process that feeds into
403 SA signaling, and therefore that these stress responses are secondary to
404 plasmodesmal closure. Further, the combined increase in sugar content and SA might
405 explain our pathoassay data; the necrotrophic pathogen *B. cinerea* might be able to
406 access increased intracellular sugar stores and be unimpeded by SA defense
407 pathways (Ferrari et al. 2003; El-Oirdi et al. 2011), while *Pst* DC3000 might be unable
408 to access intracellular sugars and is impeded by SA (Velásquez et al. 2017; Wilson et
409 al. 2017; Howlader et al. 2020). However, as inducing plasmodesmal closure still
410 enhanced resistance to *Pst* DC3000 in the SA deficient NahG×icals3m plants (Fig.
411 4d), this indicates SA is only part of plasmodesmal stress response for inducing
412 resistance.

413 Increasingly there is evidence that sugar is critical for coordinating defense in
414 *Arabidopsis*, where specific elevations in glucose-6-phosphate enhance defense
415 responses before a pathogen invasion (Yamada et a. 2024). Sugars can induce
416 specific signal transduction pathways, with some studies finding that increasing source
417 leaf carbohydrate content leads to a feedback loop of decreasing photosynthetic yield
418 (Araya et al. 2006). Additionally, an inverse relationship between plasmodesmal
419 aperture and the expression/activity of sugar transporters has been reported (Ruan et
420 al. 2001; Zhang et al. 2017; Liu et al. 2022) suggesting that cells maintain the capability
421 to transport sugars between cells by balancing plasmodesmal aperture with
422 transporter activity (Zhang et al. 2017). On this basis, we might expect that induction
423 of LexA::icals3m would activate a compensatory mechanism for sugar distribution.
424 However, we only observed that one sugar transporter was upregulated in induced
425 LexA::icals3m, SAG29/SWEET15, which is also activated by SA during the process

426 of leaf senescence (Seo et al. 2011; Wang et al. 2021a). Therefore, while this may be
427 a component of the senescing phenotype observed in induced LexA::icals3m, the
428 increased expression of this transporter does not counteract the intracellular sugar
429 accumulation observed (Chen et al. 2015). Furthermore, when we reduced the SA,
430 sugar and starch content that occurs in LexA::icals3m, impaired growth and
431 senescence still occurred (Fig. 4c and Supplementary Fig. S21). This indicates there
432 is another yet to be determined mechanism that governs these processes in response
433 to plasmodesmal closure. Irrespective, the question arises whether cellular
434 mechanisms that perceive an increase in soluble sugars are incapacitated when
435 plasmodesmata are closed and cells are isolated.

436 The variance in multiple sets of experimental data suggest that physiological
437 plasmodesmal responses are heterogeneous within a tissue, i.e., not all cells close
438 their plasmodesmata in response to an elicitor such as chitin or flg22 (Faulkner et al.
439 2013; Xu et al. 2017; Cheval et al. 2020; Tee et al. 2023b). Our transgenic lines show
440 two different patterns of plasmodesmal response: we see variability in GFP mobility in
441 the induced LexA::PD-Plug line that resembles physiological data sets despite
442 homogeneous induction of the transgene (Supplemental Fig. S1), while data from
443 induced LexA::icals3m exhibits much lower variance (Supplemental Fig. S3). This
444 suggests that LexA::icals3m induces plasmodesmal closure more homogeneously
445 than in LexA::PD-Plug, with more cells becoming isolated from their neighbors than
446 occurs physiologically. This greater homogeneity of plasmodesmal closure in
447 LexA::icals3m correlates with the responses measured in most of the assays
448 performed in this study, with effects on disease resistance, growth, ROS burst, sugar
449 and SA accumulation all greater in magnitude in, or only detected in, LexA::icals3m
450 relative to LexA::PD-Plug. Thus, our data suggests that we have detected some of
451 these effects only when they have been elicited in more cells. However, an alternative
452 possibility is that some responses to plasmodesmal closure occur only when a
453 threshold of isolated cells is reached, which would imply that responses to
454 plasmodesmal closure is a tissue level response, and that connectivity is a population-
455 level parameter. Further, that we observe homogeneous cellular isolation can result in
456 undesired outcomes suggests a degree of heterogeneity is optimal for overall
457 physiology.

458 In this study we have induced plasmodesmal closure to isolate it from other immune
459 responses and study its effects. For this to be a useful pursuit, we needed to determine
460 whether induced plasmodesmal closure mimics physiological plasmodesmal closure.
461 We reasoned that during an infection, the exposure of cells to PAMPs is likely to be a
462 sustained process suggesting that prolonged plasmodesmal closure can occur during
463 infection. This is supported by our findings that plasmodesmal callose deposits were
464 increased 72 h post *Pst hrcC*$^{-}$ infection (Supplemental Fig. S4). Beyond this, we have
465 identified that immune-independent plasmodesmal closure triggers stress-associated
466 responses, raising the question of whether these responses occur when cells are
467 isolated in any context, including developmental transitions. In many investigations of
468 developmental transitions, *icals3m* is used to induce ectopic plasmodesmal closure at
469 different cell boundaries and our data indicates that this is also likely to block the
470 distribution of sugars to, or from, targeted cells and activate defense. Thus,
471 phenotypes that arise from blocking plasmodesmata at a critical developmental
472 transition must be interpreted with these factors in mind.

473 We have found that plasmodesmal closure triggers stress responses. This suggests
474 that cellular isolation is a stress-inducing state and, conversely, that connection to
475 neighboring cells is essential for optimal growth-associated cellular functions. Thus,
476 understanding how a cell responds when it becomes isolated from its neighbors, and
477 why cell-to-cell connectivity regulates homeostatic cellular processes, is key to
478 understanding how plants function as multicellular organisms.

479

480 **Methods**

481 *Plant material*

482 All *Arabidopsis thaliana* used in this study is in the Columbia-0 ecotype background.
483 For assays on mature plants, *Arabidopsis* plants were grown at 10 h light at 22 °C, on
484 soil or for the RNA-seq experiment, on Murashige and Skoog (MS) 1% sucrose 0.8%
485 agar in 50 mm diameter petri dishes for 4–5 weeks. For MAPK and ROS measurement
486 assays on seedlings, seeds were germinated on MS 1% sucrose 0.8% agar at 16 h
487 light at 22 °C and grown for 8 days, then 10 seedlings were transferred per well on a
488 6-well plate together with 8 mL of liquid MS and grown for an additional 7 days.

489 *Confocal microscopy*

490 Microprojectile bombardment, transgene induction visualization and aniline blue
491 plasmodesmal callose measurements utilized confocal microscopy (LSM Zeiss 800).
492 RFP/mCherry was excited with a 561-nm DPSS laser and collected at 600 to 640 nm,
493 GFP/H_2DCFDA was excited with a 488-nm argon laser and collected at 505 to 530
494 nm, and aniline blue was excited with a 405-nm UV laser and collected at 430 to 550
495 nm.

496 *Microprojectile bombardment*

497 Microprojectile bombardment of *35S::GFP* was performed as described in (Tee et al.
498 2022). 24 h after DMSO or estradiol treatment, 5-week-old leaves were co-bombarded
499 with pB7WG2.0.RFP_{ER} and pB7WG2.0.GFP. Bombardment sites were then imaged
500 16 h after using confocal microscopy with a 20× water dipping objective (W N-
501 Achroplan 20×/0.5).

502 *Generation of transgenic lines and induction of transgene*

503 The *LexA::icals3m* construct is as described (Bellandi et al. 2022). The *LexA::PD-Plug*
504 construct was assembled into a binary vector via Golden Gate cloning; first the 'PD-
505 Plug' sequence was created by fusing the PDLP1 signal peptide and the PDLP1
506 transmembrane domain and cytoplasmic tail to the N- and C-termini of mCherry
507 respectively (Caillaud et al. 2014). This synthetic peptide was inserted downstream of
508 the *LexA* promoter sequence and upstream of a NOS terminator and assembled into
509 the backbone of pICSL0022013 containing the *Nos::BAR::Nos* selection cassette and
510 *Act2::XVE::Act2* cassette.

511 *LexA::PD-Plug* and *LexA::icals3m* constructs were transformed into the Col-0
512 *Arabidopsis* background and screened with phosphinothricin (10 µg/mL concentration)
513 or kanamycin selection (50 µg/mL concentration) respectively. For induction of the
514 transgene in all experiments (with the exception of size phenotyping), leaves were
515 painted on both the abaxial and adaxial side with either 0.1% DMSO (mock treatment)
516 or 20 µM β-Estradiol 17-acetate (estradiol treatment) containing 0.01% Silwet L-77 in
517 ddH_2O, using a fine paint brush. For size phenotyping, seedlings were sprayed with
518 the above specified DMSO or estradiol treatment.

519 *Plasmodesmal callose measurements*

520 24 h post treatment with either DMSO or estradiol, expanded leaves of 5-week-old
521 plants were infiltrated with 1% aniline blue in PBS buffer (pH 7.4) then imaged using
522 confocal microscopy from the abaxial side using a 63× water immersion objective
523 (Plan-Apochromat 63×/1.20). Z-stacks from multiple areas from a given treated leaf,
524 with a minimum of three biological replicates per genotype and treatment were
525 collected. An automated image analysis pipeline to quantify aniline blue-stained
526 plasmodesmata is available at (Johnston et al. 2022).

527 *Quantitative PCR*

528 To determine transgene expression, *Arabidopsis* T2 seedlings were grown on MS 1%
529 sucrose 0.8% agar with phosphinothricin (10 µg/mL concentration) or kanamycin (50
530 µg/mL concentration), for 21 days in 16 h light at 22 °C. Leaves from each line was
531 treated with DMSO or estradiol as above and harvested 48 h later in liquid nitrogen.
532 Samples were homogenized in a GenoGrinder 2100, with RNA extracted, DNase
533 treatment, first strand cDNA synthesis and qPCR performed as previously described
534 (Bellandi et al. 2022). Genes tested are *icals3m*/*CalS3* (using primers
535 AGGACGTTACTTCATGGCGG and GGCTCCGGGAATACAGTCTG) and the
536 housekeeper *AtUBQ10* (using primers AGTCTACTCTTCACTTGGTCCTGC and
537 GCCCCAAAACACAAACCACCAAAG). Normalized relative quantities (NRQs) were
538 generated using the qBase model (Hellemans et al. 2008).

539 *Pseudomonas syringae infection assays*

540 Three leaves from 4–5-week-old plants were treated with DMSO or estradiol. After 72
541 h, leaves were infiltrated with 5 × 10^4 cfu/mL *Pseudomonas syringae* DC3000 and
542 harvested 72 h later. Each leaf was harvested with a 5 mm corer and the three leaves
543 from a single plant combined as a sample. Leaf tissue was homogenized with 1 mL
544 ddH_2O for 2 mins at 1200 rpm in a GenoGrinder 2100. 5 µL of multiple 10-fold dilutions
545 were plated out with three technical replicates per plant sample, then incubated for 48
546 h at 28 °C with colony counts determined from countable dilutions. Four independent
547 experiments with five plants per treatment/genotype per experiment was performed.

548 To determine plasmodesmal associated callose deposits after *Pseudomonas syringae*
549 DC3000 *hrcC*$^-$ (*hrcC*$^-$) infection, a culture at an OD of 0.2 was prepared. Leaves from
550 5-week-old Col-0 plants were infiltrated either with H_2O (mock) or *hrcC*$^-$, and then
551 imaged 24 h, 48 h or 72 h post treatment. Aniline blue staining was performed as per

552 the above plasmodesmal callose measurements with the exception that 0.1% aniline
553 blue was used. 3-4 z-stacks from multiple areas per leaf was performed, with eight
554 biological replicates per treatment/timepoint collected. Only callose deposits at
555 plasmodesmata were analyzed.

556 *Botrytis cinerea infection assays*

557 *B. cinerea* spores were applied to leaves from 4–5-week-old plants 72 h post DMSO
558 or estradiol treatment. *B. cinerea* spores were harvested and adjusted to a
559 concentration of 2.5×10^5 spores/mL in 0.25× potato dextrose broth and incubated at
560 room temperature for 2 h with continual shaking for spore germination. Leaves were
561 adhered to 1.5% agar H_2O plates, and droplets of 2 µL spore suspensions were placed
562 in between the mid vein and leaf edge on each side. Plates were sealed with parafilm
563 and incubated in a cabinet set at 22 °C with 10 h light. Developing disease lesions
564 were photographed 2 dpi and measured using FIJI. Each prepared plate had four
565 leaves per genotype and treatment, and the average lesion area was calculated per
566 genotype/treatment in a given plate, defined as a single biological replicate. Three
567 independent experiments were conducted with a minimum of five biological replicates
568 per genotype/treatment.

569 *MAPK activation assays*

570 MAPK activation assays were performed on leaf discs from expanded leaves of 5-
571 week-old plants or on 15-day-old seedlings 72 h post treatment with DMSO or
572 estradiol. Samples were harvested 0, 5 mins, 15 mins, 30 mins and 45 mins post 100
573 nM flg22 treatment, and flash frozen in liquid nitrogen. Frozen samples were
574 homogenized via 90 seconds of shaking (1100 rpm) in a GenoGrinder 2100, then 500
575 µL protein extraction buffer (50 mM Tris-HCl pH 7.5, 150 mM NaCl, 1 mM EDTA pH
576 8.0, 10% glycerol, 0.5% NP40 IGEPAL® CA-630, protease inhibitor cocktail (Sigma)
577 1:100, phosphatase inhibitor (Sigma) 1:200, 1 mM $Na_2MoO_4 \times 2H_2O$, 1mM NaF, 1.5
578 mM activated Na_3VO_4, 5 mM DTT, 1mM PMSF) was added and the sample left to mix
579 for 30 mins at 4 °C. Samples were centrifuged at max speed for 10 mins at 4 °C,
580 supernatant transferred to a new tube and re-centrifuged at max speed for another 10
581 mins at 4 °C. The resulting supernatant was incubated at 95 °C for 15 mins with
582 Laemmli buffer, then proteins were separated by SDS-PAGE and transferred to

583 Immuno-blot® PVDF membrane. Proteins were detected using p44/42 MAPK (1:2000;
584 Cell Signaling Technologies, #9102) and α-Rabbit-HRP (1:10000, Sigma, A0545).

585 *ROS burst measurements*

586 ROS assays were performed on leaf discs taken from 5-week-old plants or 15-day-old
587 seedlings 72 h post DMSO or estradiol treatment. Leaf discs were first floated on H_2O
588 overnight; the following day water was removed, then 20 µg/mL HRP and 6 µM L-012
589 was added, with or without 100 nm flg22. The same was performed for seedlings
590 except liquid media was removed before adding the HRP and L-012.
591 Chemiluminescence was recorded using a Varioskan Flash (Thermo Fisher) over 45
592 mins, with the total luminescence emitted used for analysis.

593 *General ROS quantification*

594 20 µM H_2DCFDA (Thermo Fisher) was syringe infiltrated into expanded leaves of 5-
595 week-old plants 72 h post DMSO or estradiol treatment, and confocal microscopy was
596 performed on the abaxial side of the leaf. Z-stacks were taken from four areas of a
597 given leaf from four plants per genotype/treatment. Quantification of fluorescence was
598 performed in FIJI using a sum projection.

599 *RNA-seq*

600 Two mature leaves per 5-week-old plant were DMSO or estradiol treated, and
601 harvested 12 h, 24 h, 48 h and 72 h post treatment. Each biological replicate contained
602 four plants (i.e., 8 leaves), with three biological replicates for each
603 genotype/treatment/time point. Leaves were flash frozen in liquid nitrogen, then
604 homogenized via 90 seconds of shaking (1100 rpm) in a 2100 Geno/Grinder (Spex
605 SamplePrep, USA). Total RNA was extracted using the RNEasy Plant Mini Kit
606 (QIAGEN, Germany) and eluted into 60 µl of water. Purified RNA was treated with the
607 TURBO DNA-free kit (Thermo Fisher, USA). RNA quantification and library
608 construction was conducted by Novogene Co., Ltd (Beijing). RNA quality and quantity
609 were access via 1% agarose gel, NanoPhotometer ® spectrophotometer (IMPLEN,
610 USA), and the RNA Nano 6000 Assay Kit for the Bioanalyzer 2100 System (Agilent
611 Technologies, USA). Libraries were constructed using 0.4 µg of RNA and the
612 NEBNext ® UltraTM RNA Library Prep Kity for Illumina (NEB, USA). mRNA was
613 purified via poly-T magnetic beads. Fragmentation, cDNA synthesis, and NEBNext

614 Adaptor hybridization were performed according to manufacturer's instructions and
615 purified with the AMPure XP system (Beckman Coulter, USA). Index-coded samples
616 were clustered on a cBot Cluster Generation System using TruSeq PE Cluster Kit v3-
617 cBot-HS (Illumina, USA) and sequenced on an Illumina Novaseq platform to generate
618 150bp paired-end reads with a sequencing depth of 10 million reads per sample. All
619 sequencing data are available on GEO at GSE248301.
620
621 *Bioinformatic analyses*

622 Adaptors and low-quality (phred33<20) reads were trimmed from the data using
623 TrimGalore v0.5.0 (Krueger et al. 2021) and Cutadapt v1.7 (Martin 2011). RNA quality
624 was accessed using FastQC v0.11.8 (Babraham Bioinformatics - FastQC A Quality
625 Control tool for High Throughput Sequence Data) and MultiQC v.1.7 (Ewels et al.
626 2016). The data was mapped against the *Arabidopsis* reference genome (TAIR10;
627 NCBI Refseq GCA_000001735.1) using HISAT2 v2.1.0 (Kim et al. 2019). Mapped
628 reads were sorted using Samtools v1.4.1 Sort (Danecek et al. 2021). Transcript
629 assembly was completed using Stringtie v1.3.3 (Pertea et al. 2015) and gene counts
630 (see Supplemental Data Set 3 and 11 for gene count matrix and metadata
631 respectively) were extracted using the built-in python wrapper, prepDE.py available at
632 http://ccb.jhu.edu/software/stringtie/dl/prepDE.py. Principle component analysis was
633 conducted using DEseq2, ggplot2 (Wickham 2016), ggConvexHull, and TidyVerse
634 (Wickham et al. 2019) in R (R Core Team 2022). Differentially expressed genes were
635 determined using DEseq2 (Love et al. 2014) in R. Genes with less than 10 counts
636 across all samples were excluded from the analysis. The data was subset by
637 timepoints, and Wald Tests or Likelihood Ratio Tests (LRT) were performed based on
638 comparisons of interest. Wald Tests were used to extract DEGs based on differences
639 between treatment or genotype. LRT were used to extract genes differentially
640 expressed based on difference between closed plasmodesmata (induced/estradiol
641 treated LexA::PD-Plug and LexA::icals3m combined) and open plasmodesmata
642 (uninduced/DMSO treated LexA::PD-Plug, uninduced/DMSO treated LexA::icals3m,
643 and DMSO and estradiol treated Col-0). LRT was used in this way to determine genes
644 uniquely up- or down-regulated in the inducible lines treated with estradiol.
645 Differentially expressed genes from the Wald Test were designated if the log2 fold
646 change (lfc) was greater than |1.5| and adjusted p-value<0.05. Differentially expressed

647 genes from the LRT were considered significant if the adjusted p-value was less than
648 0.05. LRT significantly differentially expressed genes were clustered using Lasso2
649 (Lokhorst et al. 2021) and DEGreports v1.36.0 (Pantano 2023) and normalized read
650 counts plotted using ggplot2 and pheatmaps v1.0.12 (Kolde 2019). Genes involved in
651 Salicylic Acid biosynthesis/catabolism and response were determined based on a
652 Wald Test of open plasmodesmata versus closed plasmodesmata with a lfc cut-off of
653 +/-0.5 and adjusted p-value of 0.05 (Supplemental Data Set 12). Gene ontology
654 enrichment analysis was conducted based on differentially expressed genes.
655 Enrichment was conducted in TopGo v2.52.0 (Alexa and Rahnenfuhrer 2023) based
656 on TAIR10 GO terms, with a topgoFisher cut-off of $p<0.05$. GO terms were plotted in
657 ggplot2. GO parent terms were determined using the Revigo's (Supek et al. 2011)
658 redundancy feature (cut-off 0.7) and utilized to extract defense-specific enriched GO
659 terms.

660 *Transgene Mapping*

661 Transgenes were mapped by generating a pseudo-genome consisting of the
662 *Arabidopsis* TAIR genome as well as the transgene of interest (mCherry) using SeqKit
663 v0.9.1 (Shen et al. 2016) and STAR v2.5a (Dobin et al. 2013). The reads were then
664 mapped and sorted by coordinates to the pseudo-genome using STAR v2.5a. The
665 data was processed the same as previously described using Samtools and Stringtie.
666 Gene counts of mCherry (Supplemental Data Set 13) and CalS3 (Supplemental Data
667 Set 14) were extracted using DESeq2 and plotted in ggplot2.

668 *Size phenotyping*

669 9-day-old seedlings of Col-0, LexA::PD-Plug and LexA:: icals3m were finely sprayed
670 with treatments DMSO or estradiol and 6 days later, the first two true leaves were
671 adhered to a microscope slide and images taken on a Leica M205 FA stereo
672 microscope. Leaf area was measured using FIJI. For the shade experiments, 10-day-
673 old seedlings of Col-0, LexA::icals3m, NahG and NahG×icals3m were finely sprayed
674 with treatments of DMSO or estradiol and either kept at normal light conditions (80
675 $\mu mol/m^{-2}/s^{-1}$) or a shaded lid was placed on top reducing the light intensity to 9 $\mu mol/m^{-}$
676 $^{2}/s^{-1}$. An additional spray was performed 7 days post the initial treatment, and 14 days
677 post treatment the first two true leaves were adhered to a microscope slide and images
678 taken on a Axio Zoom V16 light microscope. A leaf measurement macro developed

679 using FIJI was used to measure the leaf area; the average between the two true leaves
680 per plant was calculated, and the relative size was calculated by dividing the average
681 of the DMSO control in each condition/genotype for each sample.

682 *Sugar and starch measurements*

683 Leaf tissue was harvested in liquid nitrogen from plants 72 h post treatment of either
684 DMSO or estradiol (3 leaves from 5-week-old plants), with sugars and starch
685 separately extracted from approximately 100 mg total leaf tissue as described by
686 (Smith and Zeeman 2006). Frozen tissue was homogenized for 2 mins at 1200 rpm in
687 a GenoGrinder 2100. Samples were further homogenized in 1 mL of 0.7 M cold
688 perchloric acid and then centrifuge at max speed 4 °C for 5 min. The supernatant was
689 transferred to process for sugar, while the pellet was kept on ice for starch
690 quantification. For sugar, 600 µL supernatant was transferred to a new 1.5 mL tube,
691 and neutralization buffer (2 M KOH, 400 mM MES) was added to achieve a pH of 6-7.
692 The sample was then spun at max speed for 4 min and supernatant recovered. Soluble
693 sugars were quantified by enzymatic assay in technical triplicates by monitoring NADH
694 production absorbance at 340 nm in a 96-well format using an Omega FLUOstar
695 microplate reader. Each sample was added to 50 µL of buffer (50 mM HEPES NaOH
696 pH 7.4-7.6, 1 mM $MgCl_2$, 1mM ATP, 1 mM NAD, 1.4 U Hexokinase), topped with H_2O
697 to a total volume of 198 µL. An initial A_{340} reading was taken, before adding glucose-
698 6-phosphate dehydrogenase for a kinetic reading to determine glucose content,
699 followed by adding phosphoglucose isomerase to determine fructose content, followed
700 by invertase to determine sucrose content. To determine starch content, the sample
701 pellet was first washed by adding 1 mL H_2O and vortexing, followed by centrifugation
702 for 3 mins at 3,000 ×g. Supernatant was removed, then pellet washed again by adding
703 1 mL 80% ethanol and vortexing, followed by centrifugation for 3 mins at 3,000 ×g;
704 this ethanol wash was repeated for a total of three washes. Excess ethanol was
705 evaporated, then resuspended with 750 µL of H_2O. 2 × 200 µL of each sample was
706 transferred to a new screw cap tube and incubated at 95 °C for 12 minutes. The
707 samples were left to briefly cool to room temperature (~5 min), then one aliquot was
708 digested by incubation with α-amylase (10 U) and amyloglucosidase (1.26 U) in 0.1045
709 M sodium acetate buffer (pH 4.8) for two hours at 37 °C, alongside the other aliquot
710 serving as the non-digested control (i.e., containing only the 0.1045 M sodium acetate
711 buffer and two hour 37 °C incubation). Starch content was quantified through

712 enzymatic assay of the digested aliquot sample by monitoring NADH production as
713 per the above glucose measurement. Technical triplicates were performed for each
714 digested sample, alongside a single technical replicate for the non-digested sample.
715 Starch content was calculated from the glucose assay values in mg per gram of fresh
716 weight of sample.

717 *Hormone measurements*

718 Leaves from 5-week-old plants were treated with DMSO or estradiol and harvested 72
719 h post treatment and flash frozen in liquid nitrogen; per biological replicate, a minimum
720 of six leaves from a minimum of three plants were pooled together to obtain between
721 150-220mg of fresh tissue weight. Frozen tissue was homogenized for 2 × 2 mins at
722 1200 rpm in a GenoGrinder 2100. 300 µL of buffer (10% methanol, 1% acetic acid in
723 H_2O) containing an internal standard of 1 µM salicylic acid-d_4 (SA-$_{d4}$, Merck) and 500
724 nM jasmonic acid-d_5 (JA$_{-d5}$, Cayman Chemicals) was added, mixed well with a vortex
725 then left to mix at 4 °C for 20 mins. Samples were centrifuged for 25 mins at 4°C at
726 15,000 RCF, and the supernatant recovered. The pellet was re-extracted with another
727 300 µL buffer without the internal standard, mixed and centrifuged as before, with the
728 resulting supernatant combined with the first recovered supernatant. The total
729 supernatant was centrifuged at 4 °C for 10 mins at max speed, and each sample was
730 then run for analysis. Quantification was performed on an Acquity UPLC attached to
731 a Xevo TQS tandem mass spectrometer (Waters). Separation was on a 50×2.1mm
732 2.6µM Kinetex EVO C18 column (Phenomenex) using the following gradient of
733 acetonitrile (solvent B) versus 0.1% formic acid in water (solvent A), run at 600 µL.min-
734 1 and 35°C: 0 min, 10% B; 2 min, 80% B; 2.15 min, 80% B; 2.2 min, 10% B; 3.4 min,
735 10% B. The injection volume was 5 µL. Salicylate was quantified by negative mode
736 electrospray, monitoring the transition *m/z* 137→65 (and for the internal standard the
737 corresponding transition 141→97) while jasmonate was monitored at the transition *mz*
738 209→59 (and for the internal standard the corresponding transition 214→62) at 16V
739 collision energy. Spray chamber conditions were 1.5kV spray voltage, 500°C
740 desolvation temperature, 900 $L.hr^{-1}$ desolvation gas, 150 $L.hr^{-1}$ cone gas, and 7 bar
741 nebulizer pressure. Results were processed using TargetLynx software V4.1 SCN876
742 (2012).

743 *Chlorophyll fluorescence measurements*

744 Chlorophyll fluorescence measurements were performed using an Imaging-PAM
745 chlorophyll fluorometer and ImagingWin software application (Walz). The effective
746 PSII quantum yield as indicated by Y(II) was taken following a 30 min dark adaptation
747 of leaves from 5-week-old plants 72 h post DMSO or estradiol treatment. Four leaves
748 per treatment/genotype were measured in a given run, with 8 runs in total over two
749 independent experiments.

750 *Statistical analyses*

751 Statistical analyses were performed using RStudio 2021.09.01 Build 351/R version
752 4.0.3. Data presented as boxplots have the middle line indicating the median, the box
753 representing the upper and lower quartiles, and the whiskers indicating the minimum
754 and maximum values with 1.5× interquartile range. For bootstrap analyses, data were
755 analyzed using *medianBootstrap* (Johnston and Faulkner 2021) or *medianBootstrap2*
756 (Tee et al. 2023a). Pathoassays, basal ROS quantification, and chlorophyll
757 fluorescence measurements were analyzed using a linear-mixed effects model using
758 the R package, *lmerTest*. For pathoassays the random effect was 'independent
759 experiment repeat'; for the basal ROS quantification the random effect was 'biological
760 replicate'; for chlorophyll fluorescence measurements the random effect was
761 'experimental run'. Size phenotyping, starch, sucrose, glucose and fructose
762 measurements were analyzed using a linear model. All ANOVAs specified are ANOVA
763 Satterthwaite's Method, and significant differences between factors were determined
764 by post hoc Tukey HSD using the R package, *emmeans*. Salicylic acid quantification
765 was analyzed using a Mann-Whitney test.

766

767 **Data availability**

768 Raw counts for bombardment data generated for this study (Fig. 1C and Supplemental
769 Fig. S3) is available in Supplemental Data Set 1. Additional raw counts for
770 bombardment data for Supplemental Fig. S3 are sourced from Cheval et al. 2020 and
771 Tee et al. 2023b. RNAseq data has been deposited in the Gene Expression Omnibus
772 under the accession code GSE248301, with further analysis included in Supplemental
773 Data Sets as specified in-text.

774

775 **Supplemental Data Sets**

776 Supplemental Data Set 1: Data for number of cells showing GFP within a
777 genotype/treatment

778 Supplemental Data Set 2: Background response to estradiol: differentially regulated
779 genes in response to estradiol treatment shared across all genotypes

780 Supplemental Data Set 3: Gene count matrix from the RNAseq analysis

781 Supplemental Data Set 4: Genes differentially expressed in category specified,
782 identified by a likelihood ratio test analysis

783 Supplemental Data Set 5: Genes differentially expressed in response to 12h
784 plasmodesmal closure identified by a likelihood ratio test analysis

785 Supplemental Data Set 6: Genes differentially expressed in response to 24h
786 plasmodesmal closure identified by a likelihood ratio test analysis

787 Supplemental Data Set 7: Genes differentially expressed in response to 48 h
788 plasmodesmal closure identified by a likelihood ratio test analysis

789 Supplemental Data Set 8: Genes differentially expressed in response to 72h
790 plasmodesmal closure identified by a likelihood ratio test analysis

791 Supplemental Data Set 9: Genes identified from the literature as associated with
792 salicylic acid biosynthesis, catabolism and response

793 Supplemental Data Set 10: Genes identified from the literature as associated with the
794 synthesis and transport of soluble sugars and starch

795 Supplemental Data Set 11: Metadata related to the gene count matrix

796 Supplemental Data Set 12: Log2 fold change of genes associated with SA that are
797 differentially expressed at 12h, 24h, 48h and 72h

798 Supplemental Data Set 13: Gene counts of mCherry from pseudo-genome GEO
799 GSE248301

800 Supplemental Data Set 14: Gene counts of CalS3 from pseudo-genome GEO
801 GSE248301

802

Author Contributions

CREDIT authorship breakdown:

Conceptualization – all authors

Data curation – EET, ABr, DP, HRT

Formal analysis – EET, ABr, DP, HRT

Funding acquisition – CF

Investigation – EET, ABr, DP, HRT, CW, ABe

Methodology – EET, ABr, DP, HRT, CW, ABe, CF

Project administration – CF

Resources – DP, ABr, CF

Supervision – CF

Validation – EET, ABr, DP, HRT

Visualization – EET, ABr, DP, HRT

Writing – original draft – EET, HRT, CF

Writing – review & editing – EET, ABr, DP, HRT, CW, ABe, CF

Disclosure and competing interests statement

The authors declare no competing interests.

Acknowledgements

We acknowledge access to the John Innes Centre Biomolecular Analysis Facility and thank Dr. Lionel Hill for their assistance and training with mass spectrometry, as well as access to the John Innes Centre Bioimaging Facility and thank Dr Sergio G Lopez for support with imaging. We acknowledge the Seung lab for technical assistance in the sugar and starch measurements. We would like to thank Qi Yang Ngai for their assistance in developing the leaf measurement macro and Núria Real-Tortosa for

829 critical reading of the manuscript. The *NahG* seeds were kindly provided by Jurriann
830 Ton (The University of Sheffield).

831 Work in the Faulkner lab is funded by the Biotechnology and Biological Science
832 Research Council (Grants: BB/X010996/1 and BB/X007685/1) and the European
833 Research Council (Grant: 725459 - “INTERCELLAR).

834

835

836 **References**

837 Abt MR and Zeeman SC. Evolutionary innovations in starch metabolism. Curr Opin
838 Plant Biol. 2020:55:109–117. https://doi.org/10.1016/J.PBI.2020.03.001

839 Alazem M and Burch-Smith TM. Roles of ROS and redox in regulating cell-to-cell
840 communication: Spotlight on viral modulation of redox for local spread. Plant
841 Cell Environ. 2024. https://doi.org/10.1111/PCE.14805

842 Alexa A and Rahnenfuhrer J. topGO: Enrichment Analysis for Gene Ontology. 2023.

843 Araya T, Noguchi K, and Terashima I. Effects of Carbohydrate Accumulation on
844 Photosynthesis Differ between Sink and Source Leaves of Phaseolus vulgaris
845 L. Plant Cell Physiol. 2006:47(5):644–652.
846 https://doi.org/10.1093/PCP/PCJ033

847 Aung K, Kim P, Li Z, Joe A, Kvitko B, Alfano JR. and He SY. 2020. Pathogenic bacteria
848 target plant plasmodesmata to colonize and invade surrounding tissues. *The*
849 *Plant Cell*, *32*(3), pp.595-611. https://doi.org/10.1105/tpc.19.00707

850 Babraham Bioinformatics - FastQC A Quality Control tool for High Throughput
851 Sequence Data. https://www.bioinformatics.babraham.ac.uk/projects/fastqc/.
852 Retrieved July 28, 2023

853 Bavnhøj L, Driller JH, Zuzic L, Stange AD, Schiøtt B, and Pedersen BP. Structure and
854 sucrose binding mechanism of the plant SUC1 sucrose transporter. Nature
855 Plants 2023 9:6. 2023:9(6):938–950. https://doi.org/10.1038/s41477-023-
856 01421-0

857 Beaugelin I, Chevalier A, d'Alessandro S, Ksas B, and Havaux M. (2020). Endoplasmic
858 reticulum-mediated unfolded protein response is an integral part of singlet
859 oxygen signalling in plants. The Plant Journal, 102(6), 1266-1280.
860 https://doi.org/10.1111/tpj.14700.

861 Bellandi A, Papp D, Breakspear A, Joyce J, Johnston MG, de Keijzer J, Raven EC,
862 Ohtsu M, Vincent TR, Miller AJ, et al. Diffusion and bulk flow of amino acids
863 mediate calcium waves in plants. Sci Adv. 2022:8(42):6693. DOI:
864 10.1126/sciadv.abo6693.

865 van Butselaar T and Van den Ackerveken G. Salicylic Acid Steers the Growth–
866 Immunity Tradeoff. Trends Plant Sci. 2020:25(6):566–576.
867 https://doi.org/10.1016/J.TPLANTS.2020.02.002

868 Büttner M and Sauer N. Monosaccharide transporters in plants: structure, function and
869 physiology. Biochimica et Biophysica Acta (BBA) - Biomembranes.
870 2000:1465(1–2):263–274. https://doi.org/10.1016/S0005-2736(00)00143-7

871 Caillaud MC, Wirthmueller L, Sklenar J, Findlay K, Piquerez SJM, Jones AME,
872 Robatzek S, Jones JDG, and Faulkner C. The Plasmodesmal Protein PDLP1
873 Localises to Haustoria-Associated Membranes during Downy Mildew Infection
874 and Regulates Callose Deposition. PLoS Pathog. 2014:10(11):e1004496.
875 https://doi.org/10.1371/JOURNAL.PPAT.1004496

876 Chen LQ, Hou BH, Lalonde S, Takanaga H, Hartung ML, Qu XQ, Guo WJ, Kim JG,
877 Underwood W, Chaudhuri B, et al. Sugar transporters for intercellular exchange
878 and nutrition of pathogens. Nature 2010 468:7323. 2010:468(7323):527–532.
879 https://doi.org/10.1038/nature09606

880 Chen LQ, Lin IW, Qu XQ, Sosso D, McFarlane HE, Londoño A, Samuels AL, and
881 Frommer WB. A Cascade of Sequentially Expressed Sucrose Transporters in
882 the Seed Coat and Endosperm Provides Nutrition for the Arabidopsis Embryo.
883 Plant Cell. 2015:27(3):607–619. https://doi.org/10.1105/TPC.114.134585

884 Cheval C, Samwald S, Johnston MG, Keijzer J de, Breakspear A, Liu X, Bellandi A,
885 Kadota Y, Zipfel C, and Faulkner C. Chitin perception in plasmodesmata
886 characterizes submembrane immune-signaling specificity in plants. Proc Natl
887 Acad Sci U S A. 2020:117(17):9621–9629.
888 https://doi.org/10.1073/PNAS.1907799117

889 Danecek P, Bonfield JK, Liddle J, Marshall J, Ohan V, Pollard MO, Whitwham A,
890 Keane T, McCarthy SA, and Davies RM. Twelve years of SAMtools and
891 BCFtools. Gigascience. 2021:10(2):1–4.
892 https://doi.org/10.1093/GIGASCIENCE/GIAB008

893 David LC, Lee SK, Bruderer E, Abt MR, Fischer-Stettler M, Tschopp MA, Solhaug EM,
894 Sanchez K, and Zeeman SC. BETA-AMYLASE9 is a plastidial nonenzymatic
895 regulator of leaf starch degradation. Plant Physiol. 2022:188(1):191–207.
896 https://doi.org/10.1093/PLPHYS/KIAB468

897 Delaney TP, Uknes S, Vernooij B, Friedrich L, Weymann K, Negrotto D, Gaffney T,
898 Gut-Rella M, Kessmann H, Ward E, et al. A central role of salicylic acid in plant
899 disease resistance. Science. 1994:266(5188):1247–1250.
900 https://doi.org/10.1126/SCIENCE.266.5188.1247

901 Dobin A, Davis CA, Schlesinger F, Drenkow J, Zaleski C, Jha S, Batut P, Chaisson M,
902 and Gingeras TR. STAR: ultrafast universal RNA-seq aligner. Bioinformatics.
903 2013:29(1):15–21. https://doi.org/10.1093/BIOINFORMATICS/BTS635

904 El-Oirdi M, El-Rahman TA, Rigano L, El-Hadrami A, Rodriguez MC, Daayf F, Vojnov
905 A, and Bouarab K. Botrytis cinerea Manipulates the Antagonistic Effects
906 between Immune Pathways to Promote Disease Development in Tomato. Plant
907 Cell. 2011:23(6):2405. https://doi.org/10.1105/TPC.111.083394

908 Ewels P, Magnusson M, Lundin S, and Käller M. MultiQC: summarize analysis results
909 for multiple tools and samples in a single report. Bioinformatics.
910 2016:32(19):3047–3048. https://doi.org/10.1093/BIOINFORMATICS/BTW354

911 Faulkner C, Petutschnig E, Benitez-Alfonso Y, Beck M, Robatzek S, Lipka V, and
912 Maule AJ. LYM2-dependent chitin perception limits molecular flux via
913 plasmodesmata. Proc Natl Acad Sci U S A. 2013:110(22):9166–9170.
914 https://doi.org/10.1073/PNAS.1203458110/-/DCSUPPLEMENTAL

915 Ferrari S, Plotnikova JM, De Lorenzo G, and Ausubel FM. Arabidopsis local resistance
916 to Botrytis cinerea involves salicylic acid and camalexin and requires EDS4 and

917 PAD2, but not SID2, EDS5 or PAD4. The Plant Journal. 2003:35(2):193–205.
918 https://doi.org/10.1046/J.1365-313X.2003.01794.X

919 Friedrich L, Vernooij B, Gaffney T, Morse A, and Ryals J. Characterization of tobacco
920 plants expressing a bacterial salicylate hydroxylase gene. Plant Mol Biol.
921 1995:29(5):959–968. https://doi.org/10.1007/BF00014969/METRICS

922 Gaffney T, Friedrich L, Vernooij B, Negrotto D, Nye G, Uknes S, Ward E, Kessmann
923 H, and Ryals J. Requirement of Salicylic Acid for the Induction of Systemic
924 Acquired Resistance. Science. 1993:261(5122):754–756.
925 https://doi.org/10.1126/SCIENCE.261.5122.754

926 German L, Yeshvekar R, and Benitez-Alfonso Y. Callose metabolism and the
927 regulation of cell walls and plasmodesmata during plant mutualistic and
928 pathogenic interactions. Plant Cell Environ. 2023:46(2):391–404.
929 https://doi.org/10.1111/PCE.14510

930 Hellemans J, Mortier G, De Paepe A, Speleman F, and Vandesompele J. qBase
931 relative quantification framework and software for management and automated
932 analysis of real-time quantitative PCR data. Genome Biol. 2008:8(2):1–14.
933 https://doi.org/10.1186/GB-2007-8-2-R19/COMMENTS

934 Howlader P, Bose SK, Jia X, Zhang C, Wang W, and Yin H. Oligogalacturonides
935 induce resistance in Arabidopsis thaliana by triggering salicylic acid and
936 jasmonic acid pathways against Pst DC3000. Int J Biol Macromol.
937 2020:164:4054–4064. https://doi.org/10.1016/J.IJBIOMAC.2020.09.026

938 Johnson DA, Hill JP, and Thomas MA. The monosaccharide transporter gene family
939 in land plants is ancient and shows differential subfamily expression and
940 expansion across lineages. BMC Evol Biol. 2006:6(1):1–20.
941 https://doi.org/10.1186/1471-2148-6-64/FIGURES/10

942 Johnston MG, Bellandi A, and Faulkner C. faulknerfalcons/PD_detection: Toolkit for
943 quantification of callose at plasmodesmata. 2022.
944 https://doi.org/10.5281/ZENODO.6583765

945 Johnston MG and Faulkner C. A bootstrap approach is a superior statistical method
946 for the comparison of non-normal data with differing variances. New
947 Phytologist. 2021:230(1):23–26. https://doi.org/10.1111/NPH.17159

948 Kim D, Paggi JM, Park C, Bennett C, and Salzberg SL. Graph-based genome
949 alignment and genotyping with HISAT2 and HISAT-genotype. Nat Biotechnol.
950 2019:37(8):907–915. https://doi.org/10.1038/S41587-019-0201-4

951 Kolde R. Package “pheatmap.” 2019.

952 Kraner ME, Link K, Melzer M, Ekici AB, Uebe S, Tarazona P, Feussner I, Hofmann J,
953 and Sonnewald U. Choline transporter-like1 (CHER1) is crucial for
954 plasmodesmata maturation in Arabidopsis thaliana. The Plant Journal.
955 2017:89(2):394–406. https://doi.org/10.1111/TPJ.13393

956 Kronberg K, Vogel F, Rutten T, Hajirezaei MR, Sonnewald U, and Hofius D. The Silver
957 Lining of a Viral Agent: Increasing Seed Yield and Harvest Index in Arabidopsis
958 by Ectopic Expression of the Potato Leaf Roll Virus Movement Protein. Plant
959 Physiol. 2007:145(3):905–918. https://doi.org/10.1104/PP.107.102806

960 Krueger F, James F, Ewels P, Afyounian E, and Schuster-Boeckler B.
961 FelixKrueger/TrimGalore: v0.6.7 - DOI via Zenodo. 2021.
962 https://doi.org/10.5281/ZENODO.5127899

963 Law SR, Chrobok D, Juvany M, Delhomme N, Lindén P, Brouwer B, Ahad A, Moritz
964 T, Jansson BS, Gardeström P, et al. Darkened Leaves Use Different Metabolic
965 Strategies for Senescence and Survival. Plant Physiol. 2018:177(1):132–150.
966 https://doi.org/10.1104/PP.18.00062

967 Lee J-Y, Wang X, Cui W, Sager R, Modla S, Czymmek K, Zybaliov B, Wijk K van,
968 Zhang C, Lu H, et al. A Plasmodesmata-Localized Protein Mediates Crosstalk
969 between Cell-to-Cell Communication and Innate Immunity in Arabidopsis. Plant
970 Cell. 2011:23(9):3353–3373. https://doi.org/10.1105/TPC.111.087742

971 Levy A, Erlanger M, Rosenthal M, and Epel BL. A plasmodesmata-associated beta-
972 1,3-glucanase in Arabidopsis. Plant J. 2007:49(4):669–682.
973 https://doi.org/10.1111/J.1365-313X.2006.02986.X

974 Li Z, Variz H, Chen Y, Liu SL, Aung K. Plasmodesmata-Dependent Intercellular
975 Movement of Bacterial Effectors. Front Plant Sci. 2021 Mar 22;12:640277. doi:
976 10.3389/fpls.2021.640277. PMID: 33959138; PMCID: PMC8095247.

977 Li Z, Liu SL, Montes-Serey C, Walley JW, Aung K. PLASMODESMATA-LOCATED
978 PROTEIN 6 regulates plasmodesmal function in Arabidopsis vasculature. Plant
979 Cell. 2024 Jun 6:koae166. doi: 10.1093/plcell/koae166. Epub ahead of print.
980 PMID: 38842334.

981 Liu YH, Song YH, and Ruan YL. Sugar conundrum in plant–pathogen interactions:
982 roles of invertase and sugar transporters depend on pathosystems. J Exp Bot.
983 2022:73(7):1910. https://doi.org/10.1093/JXB/ERAB562

984 Lokhorst J, Venables B, and Turlach B. R package “lasso2.” 2021.
985 https://github.com/cran/lasso2. Retrieved July 28, 2023

986 Love MI, Huber W, and Anders S. Moderated estimation of fold change and dispersion
987 for RNA-seq data with DESeq2. Genome Biol. 2014:15(12):1–21.
988 https://doi.org/10.1186/S13059-014-0550-8/FIGURES/9

989 Martin M. Cutadapt removes adapter sequences from high-throughput sequencing
990 reads. EMBnet J. 2011:17(1):10–12. https://doi.org/10.14806/EJ.17.1.200

991 Monroe JD and Storm AR. Review: The Arabidopsis β-amylase (BAM) gene family:
992 Diversity of form and function. Plant Science. 2018:276:163–170.
993 https://doi.org/10.1016/J.PLANTSCI.2018.08.016

994 Ohtsu M, Jennings J, Johnston M, Breakspear A, Liu X, Stark K, Morris RJ, de Keijzer
995 J, Faulkner C. Assaying Effector Cell-to-Cell Mobility in Plant Tissues Identifies

996 Hypermobility and Indirect Manipulation of Plasmodesmata. Mol Plant Microbe
997 Interact. 2024 Feb;37(2):84-92. doi: 10.1094/MPMI-05-23-0052-TA. Epub 2024
998 Feb 26. PMID: 37942798.

999 Pantano L. DEGreport: Report of DEG analysis. 2023.
1000 https://doi.org/10.18129/B9.bioc.DEGreport

1001 Paterlini A, Dorussen D, Fichtner F, van Rongen M, Delacruz R, Vojnović A, Helariutta
1002 Y and Leyser O. (2021), Callose accumulation in specific phloem cell types
1003 reduces axillary bud growth in *Arabidopsis thaliana*. New Phytol, 231: 516-
1004 523. https://doi.org/10.1111/nph.17398

1005 Pertea M, Pertea GM, Antonescu CM, Chang TC, Mendell JT, and Salzberg SL.
1006 StringTie enables improved reconstruction of a transcriptome from RNA-seq
1007 reads. Nature Biotechnology 2015 33:3. 2015:33(3):290–295.
1008 https://doi.org/10.1038/nbt.3122

1009 Preiser AL, Banerjee A, Weise SE, Renna L, Brandizzi F, and Sharkey TD.
1010 Phosphoglucoisomerase Is an Important Regulatory Enzyme in Partitioning
1011 Carbon out of the Calvin-Benson Cycle. Front Plant Sci. 2020:11:580726.
1012 https://doi.org/10.3389/FPLS.2020.580726/BIBTEX

1013 R Core Team. R: A language and environment for statistical computing. R Foundation
1014 for Statistical Computing, Vienna, Austria. 2022. https://www.R-project.org/

1015 Ross-Elliott TJ, Jensen KH, Haaning KS, Wager BM, Knoblauch J, Howell AH,
1016 Mullendore DL, Monteith AG, Paultre D, Yan D, Otero S, Bourdon M, Sager R,
1017 Lee JY, Helariutta Y, Knoblauch M, Oparka KJ (2017) Phloem unloading in
1018 Arabidopsis roots is convective and regulated by the phloem-pole pericycle
1019 eLife 6:e24125 https://doi.org/10.7554/eLife.24125

1020 Ruan YL, Llewellyn DJ, and Furbank RT. The Control of Single-Celled Cotton Fiber
1021 Elongation by Developmentally Reversible Gating of Plasmodesmata and
1022 Coordinated Expression of Sucrose and K+ Transporters and Expansin. Plant
1023 Cell. 2001:13(1):47–60. https://doi.org/10.1105/TPC.13.1.47

1024 Seo PJ, Park JM, Kang SK, Kim SG, and Park CM. An Arabidopsis senescence-
1025 associated protein SAG29 regulates cell viability under high salinity. Planta.
1026 2011:233(1):189–200. https://doi.org/10.1007/S00425-010-1293-8

1027 Sevilem I, Miyashima S, and Helariutta Y. (2012). Cell-to-cell communication via
1028 plasmodesmata in vascular plants. Cell Adhesion & Migration. 7(1), 27–32.
1029 https://doi.org/10.4161/cam.22126

1030 Seyfferth C, Tsuda K, Lu H, and Grant M. Salicylic acid signal transduction: the
1031 initiation of biosynthesis, perception and transcriptional reprogramming. 2014.
1032 https://doi.org/10.3389/fpls.2014.00697

1033 Shen W, Le S, Li Y, and Hu F. SeqKit: A Cross-Platform and Ultrafast Toolkit for
1034 FASTA/Q File Manipulation. PLoS One. 2016:11(10):e0163962.
1035 https://doi.org/10.1371/JOURNAL.PONE.0163962

1036 Smith AM and Zeeman SC. Quantification of starch in plant tissues. Nature Protocols
1037 2006 1:3. 2006:1(3):1342–1345. https://doi.org/10.1038/nprot.2006.232

1038 Smith AM and Zeeman SC. Starch: A Flexible, Adaptable Carbon Store Coupled to
1039 Plant Growth. Annual Review of Plant Biology. 2020:71:217–245.
1040 https://doi.org/10.1146/ANNUREV-ARPLANT-050718-100241

1041 Spoel SH, Koornneef A, Claessens SMC, Korzelius JP, Van Pelt JA, Mueller MJ,
1042 Buchala AJ, Métraux JP, Brown R, Kazan K, et al. NPR1 Modulates Cross-Talk
1043 between Salicylate- and Jasmonate-Dependent Defense Pathways through a
1044 Novel Function in the Cytosol. Plant Cell. 2003:15(3):760–770.
1045 https://doi.org/10.1105/TPC.009159

1046 Supek F, Bošnjak M, Škunca N, and Šmuc T. REVIGO Summarizes and Visualizes
1047 Long Lists of Gene Ontology Terms. PLoS One. 2011:6(7):e21800.
1048 https://doi.org/10.1371/JOURNAL.PONE.0021800

1049 Tee EE, Johnston MG, and Faulkner C. faulknerfalcons/Tee-etal-2023. 2023a.
1050 https://doi.org/10.5281/ZENODO.7680790

1051 Tee EE, Johnston MG, Papp D, and Faulkner C. A PDLP-NHL3 complex integrates
1052 plasmodesmal immune signaling cascades. Proceedings of the National
1053 Academy of Sciences. 2023b:120(17):e2216397120.
1054 https://doi.org/10.1073/PNAS.2216397120

1055 Tee EE, Samwald S, and Faulkner C. Quantification of Cell-to-Cell Connectivity Using
1056 Particle Bombardment. 2022:263–272. https://doi.org/10.1007/978-1-0716-
1057 2132-5_17

1058 Thomas CL, Bayer EM, Ritzenthaler C, Fernandez-Calvino L, and Maule AJ. Specific
1059 Targeting of a Plasmodesmal Protein Affecting Cell-to-Cell Communication.
1060 PLoS Biol. 2008:6(1):e7. https://doi.org/10.1371/JOURNAL.PBIO.0060007

1061 Tomczynska I, Stumpe M, Doan TG, Mauch F. A Phytophthora effector protein
1062 promotes symplastic cell-to-cell trafficking by physical interaction with
1063 plasmodesmata-localised callose synthases. New Phytol. 2020
1064 Sep;227(5):1467-1478. doi: 10.1111/nph.16653. Epub 2020 Jun 8. PMID:
1065 32396661.

1066 Vatén A, Dettmer J, Wu S, Stierhof YD, Miyashima S, Yadav SR, Roberts CJ,
1067 Campilho A, Bulone V, Lichtenberger R, et al. Callose Biosynthesis Regulates
1068 Symplastic Trafficking during Root Development. Dev Cell. 2011:21(6):1144–
1069 1155. https://doi.org/10.1016/j.devcel.2011.10.006

1070 Velásquez AC, Oney M, Huot B, Xu S, and He SY. Diverse mechanisms of resistance
1071 to Pseudomonas syringae in a thousand natural accessions of Arabidopsis
1072 thaliana. New Phytologist. 2017:214(4):1673–1687.
1073 https://doi.org/10.1111/NPH.14517

1074 Vlot AC, Liu PP, Cameron RK, Park SW, Yang Y, Kumar D, Zhou F, Padukkavidana
1075 T, Gustafsson C, Pichersky E, et al. Identification of likely orthologs of tobacco
1076 salicylic acid-binding protein 2 and their role in systemic acquired resistance in

1077 Arabidopsis thaliana. The Plant Journal. 2008:56(3):445–456.
1078 https://doi.org/10.1111/J.1365-313X.2008.03618.X

1079 Wang C, Dai S, Zhang ZL, Lao W, Wang R, Meng X, and Zhou X. Ethylene and
1080 salicylic acid synergistically accelerate leaf senescence in Arabidopsis. J Integr
1081 Plant Biol. 2021a:63(5):828–833.
1082 https://doi.org/10.1111/JIPB.13075/SUPPINFO

1083 Wang X, Sager R, Cui W, Zhang C, Lu H, and Lee JY. Salicylic Acid Regulates
1084 Plasmodesmata Closure during Innate Immune Responses in Arabidopsis.
1085 Plant Cell. 2013:25(6):2315. https://doi.org/10.1105/TPC.113.110676

1086 Wang Y, Li X, Fan B, Zhu C, and Chen Z. Regulation and Function of Defense-Related
1087 Callose Deposition in Plants. Int J Mol Sci. 2021b:22(5):1–15.
1088 https://doi.org/10.3390/IJMS22052393

1089 Wickham H. ggplot2: Elegant Graphics for Data Analysis (Spring-Verlag New York).

1090 Wickham H, Averick M, Bryan J, Chang W, D' L, Mcgowan A, François R, Grolemund
1091 G, Hayes A, Henry L, et al. Welcome to the Tidyverse. J Open Source Softw.
1092 2019:4(43):1686. https://doi.org/10.21105/JOSS.01686

1093 Wildermuth MC, Dewdney J, Wu G, and Ausubel FM. Isochorismate synthase is
1094 required to synthesize salicylic acid for plant defence. Nature 2001 414:6863.
1095 2001:414(6863):562–565. https://doi.org/10.1038/35107108

1096 Williams LE, Lemoine R, and Sauer N. Sugar transporters in higher plants – a diversity
1097 of roles and complex regulation. Trends Plant Sci. 2000:5(7):283–290.
1098 https://doi.org/10.1016/S1360-1385(00)01681-2

1099 Wilson DC, Kempthorne CJ, Carella P, Liscombe DK, and Cameron RK. Age-related
1100 resistance in arabidopsis thaliana involves the MADS-domain transcription
1101 factor SHORT VEGETATIVE PHASE and direct action of salicylic acid on
1102 pseudomonas syringae. Molecular Plant-Microbe Interactions.
1103 2017:30(11):919–929. https://doi.org/10.1094/MPMI-07-17-0172-
1104 R/ASSET/IMAGES/LARGE/MPMI-07-17-0172-R_F8.JPEG

1105 Wu S, O'Lexy R, Xu M, Sang Y, Chen X, Yu Q, Gallagher KL. Symplastic signaling
1106 instructs cell division, cell expansion, and cell polarity in the ground tissue of
1107 Arabidopsis thaliana roots. Proc Natl Acad Sci U S A. 2016 Oct
1108 11;113(41):11621-11626. doi: 10.1073/pnas.1610358113. Epub 2016 Sep 23.
1109 PMID: 27663740; PMCID: PMC5068303.

1110 Xu B, Cheval C, Laohavisit A, Hocking B, Chiasson D, Olsson TSG, Shirasu K,
1111 Faulkner C, and Gilliham M. A calmodulin-like protein regulates plasmodesmal
1112 closure during bacterial immune responses. New Phytologist. 2017:215:77–84.
1113 https://doi.org/10.1111/nph.14599

1114 Yadav SR, Yan D, Sevilem I, Helariutta Y. Plasmodesmata-mediated intercellular
1115 signaling during plant growth and development. Front Plant Sci. 2014 Feb
1116 17;5:44. doi: 10.3389/fpls.2014.00044. PMID: 24596574; PMCID:
1117 PMC3925825.

1118 Yang L, Li B, Zheng XY, Li J, Yang M, Dong X, He G, An C, and Deng XW. Salicylic
1119 acid biosynthesis is enhanced and contributes to increased biotrophic pathogen
1120 resistance in Arabidopsis hybrids. Nature Communications 2015 6:1.
1121 2015:6(1):1–12. https://doi.org/10.1038/ncomms8309

1122 Zhang Z, Ruan YL, Zhou N, Wang F, Guan X, Fang L, Shang X, Guo W, Zhu S, and
1123 Zhang T. Suppressing a Putative Sterol Carrier Gene Reduces Plasmodesmal
1124 Permeability and Activates Sucrose Transporter Genes during Cotton Fiber
1125 Elongation. Plant Cell. 2017:29(8):2027–2046.
1126 https://doi.org/10.1105/TPC.17.00358

1127 Zhongpeng L, Liu SL, Montes-Serey C, Walley JW, and Aung K. PLASMODESMATA-
1128 LOCATED PROTEIN 6 regulates plasmodesmal function in Arabidopsis
1129 vasculature. Plant Cell. 2024 koae166. https://doi.org/10.1093/plcell/koae166

1130 Zuo J, Niu QW, and Chua NH. Technical advance: An estrogen receptor-based
1131 transactivator XVE mediates highly inducible gene expression in transgenic
1132 plants. Plant J. 2000:24(2):265–273. https://doi.org/10.1046/J.1365-
1133 313X.2000.00868.X

1134

1135 **Figures**

1136 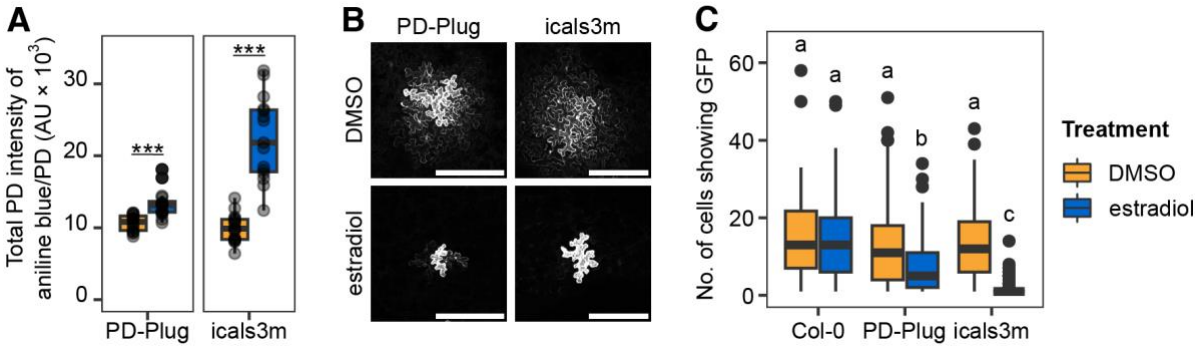

1137 **Figure 1. Characterization of plasmodesmal status in induced LexA::PD-Plug**
1138 **and LexA::icals3m tissue. A)** Quantification of aniline blue-stained plasmodesmata-
1139 associated callose in 5-week-old plants of LexA::PD-Plug (PD-Plug) or LexA::icals3m
1140 (icals3m) 24 h post DMSO or estradiol treatment. Datapoints represent the average of
1141 the total PD intensity/plasmodesmata (PD) per image, with n ≥ 14 per
1142 genotype/treatment. Bootstrap analysis indicates significant differences between
1143 DMSO and estradiol treatment in PD-Plug and icals3m, as indicated by *** $p < 0.001$.
1144 **B)** Example micrographs of bombardment sites showing movement of GFP from
1145 transformed cells indicate cell-to-cell connectivity of uninduced (DMSO) versus
1146 restricted cell connectivity in induced (estradiol) leaves of PD-Plug and icals3m. **C)**
1147 Quantification of microprojectile bombardment data showing GFP movement into
1148 neighboring cells. Leaves of 5-week-old plants were bombarded after 24 h treatment
1149 of DMSO or estradiol; n ≥ 62 bombardment sites. Bootstrap analysis with significant
1150 differences indicated by a, b and c, with $p < 0.01$. Scale bar = 200 µM.

1151

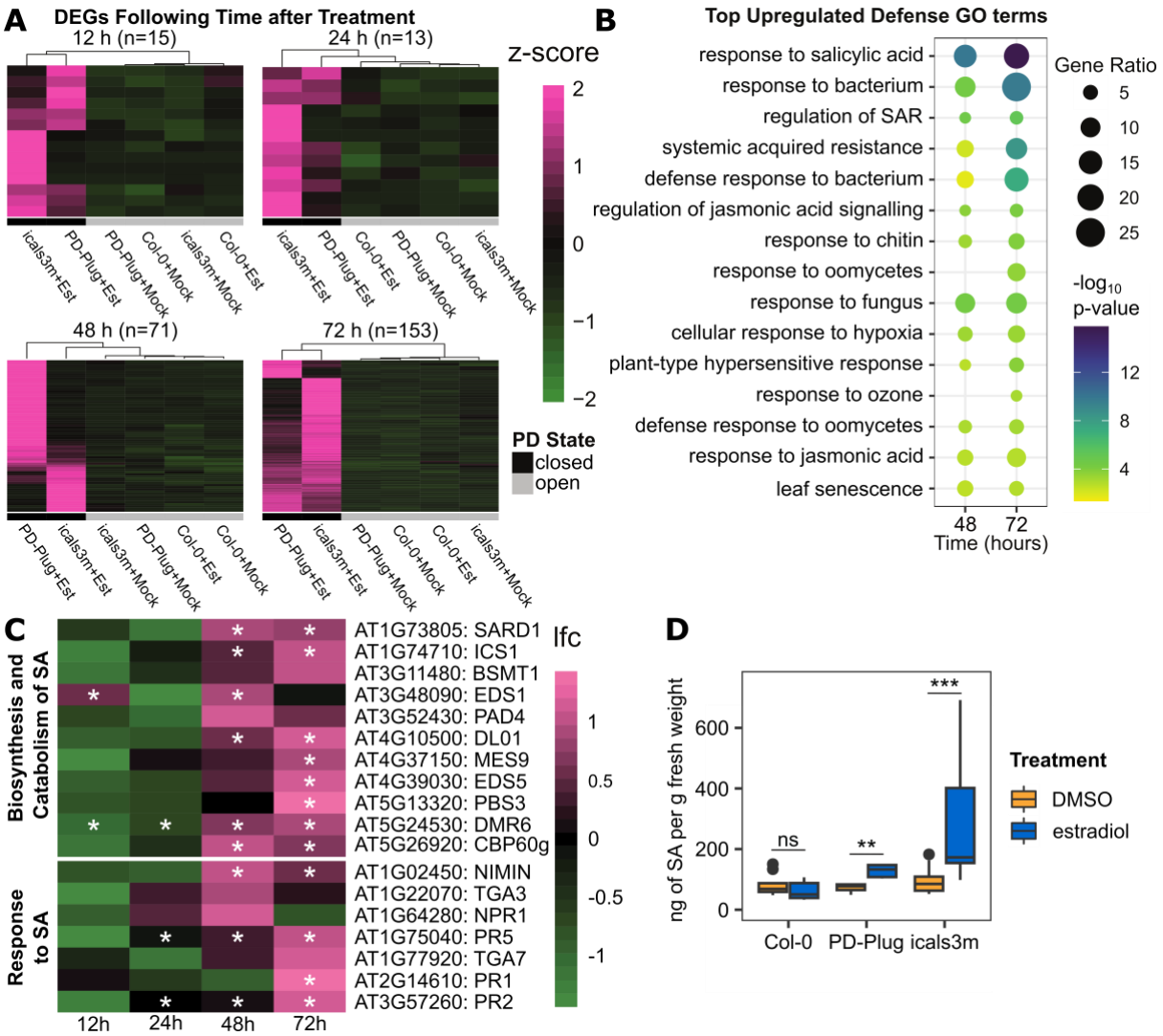

Figure 2. Plasmodesmal closure triggers stress transcriptional responses and salicylic acid related changes. A) Likelihood ratio test analysis determined number (indicated by n) of differentially expressed genes (DEGs) significantly differed between plasmodesmal status (i.e., PD State closed or open), and matches the cluster pattern of upregulated in closed state in comparison to open state at 12, 24, 48 and 72 h post treatment. Hierarchical clustering grouped together plasmodesmal state of open (i.e., estradiol treated LexA::PD-Plug and LexA::icals3m) and closed (DMSO treated LexA::PD-Plug, LexA::icals3m and Col-0, and estradiol treated Col-0). Expression normalized by row (z-score). **B)** Top 15 defense GO terms enriched over time when plasmodesmata are closed. **C)** Expression of genes related to the salicylic acid biosynthesis/catabolism and response over time when plasmodesmata are closed (i.e., in estradiol treated LexA::PD-Plug and LexA::icals3m). **D)** Quantification of salicylic acid in 5-week-old plants after 72 h DMSO or estradiol treatment, n ≥ 6 per genotype/treatment. Significant differences between treatment within a genotype analyzed using Mann-Whitney test denoted by ** $p < 0.01$, or *** $p < 0.001$.

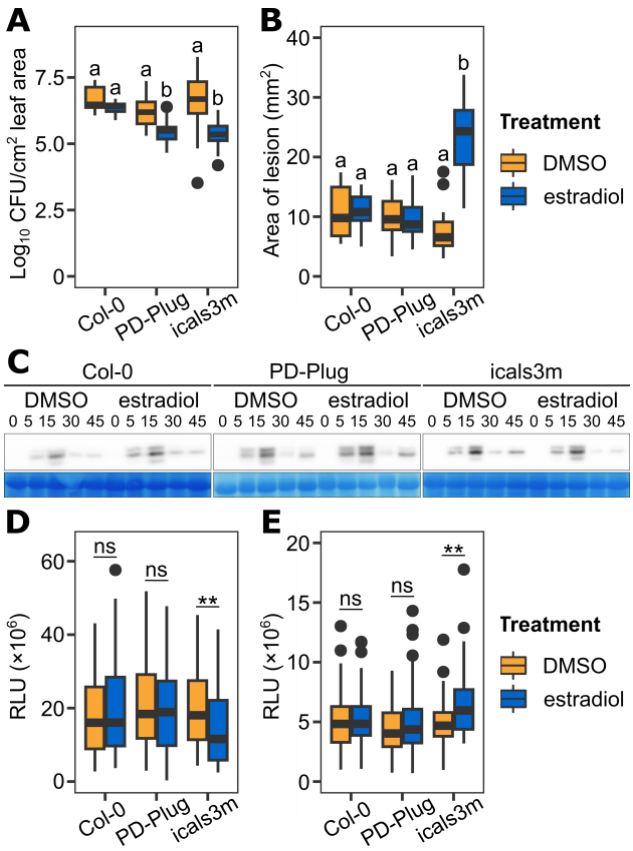

Figure 3. Plasmodesmal closure differentially impacts pathogen resistance and immune responses. A) Bacterial growth ($\log_{10}$ CFU/cm^2 leaf area) of *Pst* DC3000 3 dpi on uninduced and induced tissue of 4–5-week-old plants of Col-0, LexA::PD-Plug (PD-Plug) and LexA::icals3m (icals3m). Tissue was treated with DMSO (uninduced) or estradiol (induced) 72 h prior to infection. 4 independent experiments were conducted, with 5 plants per treatment/genotype; N = 20. Independent factors genotype and treatment were significant, with a significant interaction between the two (ANOVA; F = 16.6, df = 2, P < 0.0001; F = 67.0, df = 1, P < 0.0001; F = 8.2, df = 2, P < 0.001). Significant differences denoted by a and b, p < 0.0001. **B)** The average area of *Botrytis cinerea* disease lesions 2 dpi in leaves of 5-week-old plants of induced and uninduced Col-0, LexA::PD-Plug and LexA::icals3m. Tissue was treated with DMSO (uninduced) or estradiol (induced) 72 h prior to infection, with N = 16-17 for all genotypes/treatment combined from three independent repeats. Independent factors genotype and treatment were significant with a significant interaction between the two (ANOVA; F = 24.4, df = 2, P < 0.0001; F = 52.7, df = 1, P < 0.0001; F = 57.0, df = 2, P < 0.0001). Significant differences denoted by a and b, p < 0.0001. **C)** Western blot detection of MAPK-activation by flg22 treatment in leaf discs from expanded leaves of 4–5-week-old plants of Col-0, LexA::PD-Plug and LexA::icals3m collected 72 h post DMSO or estradiol treatment. Minute timings of tissue harvest are denoted, and Coomassie blue staining shown below as loading controls. **D)** Average relative light units (RLU) generated from ROS production in response to flg22 in leaf discs of 5-week-old plants. Leaves were treated with estradiol or DMSO 72 h prior to flg22 treatment and data is combined from two independent experiment with N = 95 per genotype/treatment. Significant differences between treatment determined by bootstrap analysis, with significant differences denoted by **, p < 0.01. **E)** Average RLU generated from ROS production in response to flg22 in seedlings. Plants were

1195 treated with estradiol or DMSO 72 h prior to flg22 treatment, with N ≥ 80 per
1196 genotype/treatment. Significant differences between treatment determined by
1197 bootstrap analysis, with significant differences denoted by **, $p < 0.01$.

1198 .

1199

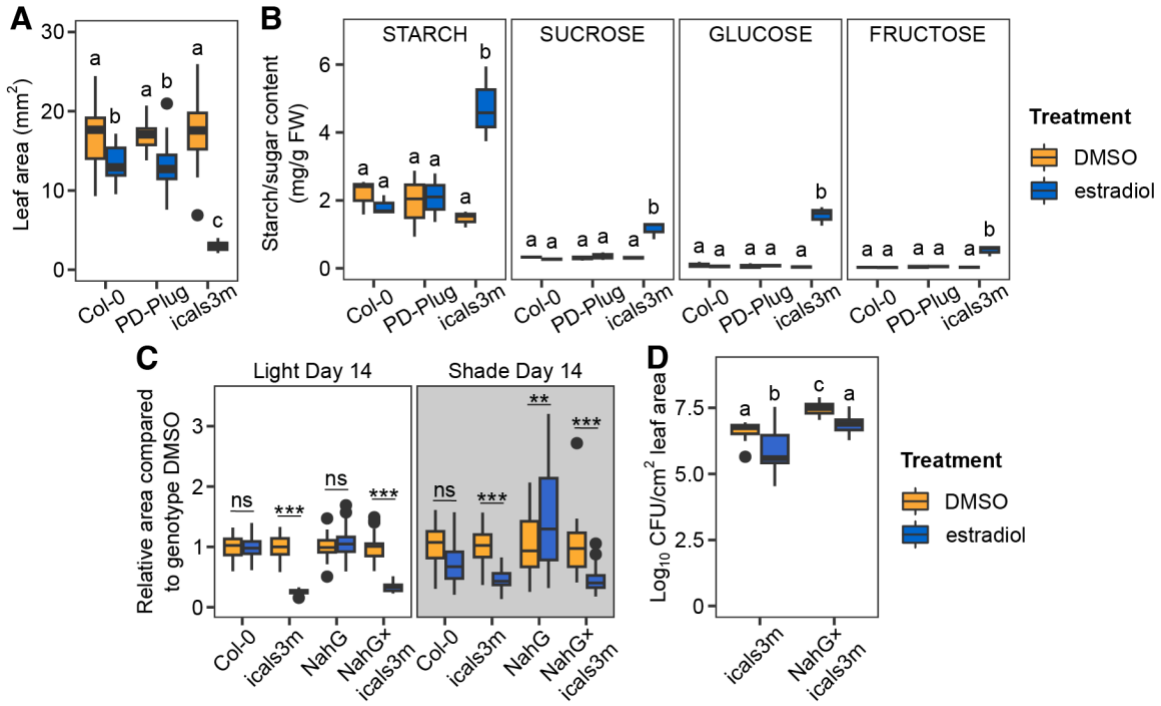

Figure 4. Plasmodesmal closure induces sugar accumulation and impairs leaf growth. A) Leaf area of first two true leaves 6 days post treatment (DMSO or estradiol) of Col-0, LexA::PD-Plug (PD-Plug) and LexA::icals3m (icals3m). Independent factors genotype and treatment were significant, with a significant interaction between the two (ANOVA; F = 82.4, df = 2, P < 0.0001; F = 445.0, df = 1, P < 0.0001; F = 104.2, df = 2, P < 0.0001). Significant differences denoted by a, b and c, p < 0.0001. n = 40. **B)** Starch, sucrose, glucose and fructose content in leaves of 5-week-old plants 72 h post DMSO or estradiol treatment. Independent factors genotype and treatment were significant, with a significant interaction between the two for each metabolite (ANOVA; *starch* F = 4.7, df = 2, P < 0.05, F = 9.2, df = 1, P < 0.05; F = 11.4, df = 2, P < 0.01; *sucrose* F = 26.2, df = 2, P < 0.0001; F = 25.8, df = 1, P < 0.001; F = 26.7, df = 2, P < 0.0001; *glucose* F = 70.0, df = 2, P < 0.0001; F = 74.4, df = 1, P < 0.0001; F = 79.3, df = 2, P < 0.0001; *fructose* F = 28.0, df = 2, P < 0.0001; F = 30.4, df = 1, P < 0.0001; F = 28.8, df = 2, P < 0.0001). Significant differences denoted by a and b, p < 0.01. **C)** Relative leaf area of true leaves 14 days post initial treatment (DMSO or estradiol) in light or shade conditions of Col-0, icals3m, NahG and NahG×LexA::icals3m (NahG×icals3m). Independent factors treatment, genotype and shade condition were significant, with a significant interaction between the pairs and all three (ANOVA; F = 105.5, df = 1, P < 0.0001; F = 84.5, df =3, P < 0.0001; F = 940.8, df = 1, P < 0.0001; F = 100.0, df = 3, P < 0.0001; F = 44.4, df = 1, P < 0.0001; F = 53.9, df = 3, P < 0.0001; F = 53.7, df = 3, P < 0.0001). Significant differences denoted by * p < 0.05, ** p < 0.01, and *** p < 0.001. **D)** Bacterial growth ($\log_{10}$ CFU/cm^2 leaf area) of *Pst* DC3000 3 dpi on uninduced and induced tissue of 4–5-week-old plants. Tissue was treated with DMSO (uninduced) or estradiol (induced) 72 h prior to infection. 4 independent experiments were conducted, with 5 plants per treatment/genotype; N = 20. Independent factors treatment and genotype were significant, with no significant interaction between the two (ANOVA; F = 42.6, df = 1, P < 0.0001; F = 75.8, df = 1, P

1228 < 0.0001; F = 0.4, df = 1, P =0.5). Significant differences denoted by a, b and c, p <
1229 0.0005.

1230

1231 **Tables**

1232 **Table 1. Photosynthetic yield as indicated by Y(II) following DMSO or estradiol**
1233 **treatment of leaves of Col-0, LexA::PD-Plug (PD-Plug) and LexA::icals3m**
1234 **(icals3m).** Pooled average of Y(II) ± SD, with a biological replicate data averaged from
1235 4 leaves per treatment/genotype on a given experimental run where N = 8, combined
1236 from two independent experiments. Independent factors genotype and treatment were
1237 not significant, with no significant interaction between the two (ANOVA; F = 1.3, df =
1238 2, P = 0.29; F = 1.2, df = 1, P = 0.29, F = 0.1, df = 2, P = 0.92).

	Col-0	PD-Plug	icals3m
DMSO	0.79±0.02	0.78±0.02	0.78±0.02
estradiol	0.79±0.01	0.78±0.01	0.79±0.01

1239

1240